# An Electrical Tomographic Approach to Detect Deformation over Soft and Flexible Materials

March  2017

Francesco Visentin

# An Electrical Tomographic Approach to Detect Deformation over Soft and Flexible Materials

Graduate School of Systems and Information Engineering

University of Tsukuba

March  2017

Francesco Visentin

# *Abstract*

In this research, we investigate, develop, and verify an approach to sense over soft and flexible materials based on the use of a tomographic technique known as Electrical Impedance Tomography. The idea has been already investigated in the field of distributed sensing but has been mostly applied to stiff geometries. In this work we want to expend its application where the underlying geometry can change its shape. The use of such capability can be beneficial in applications related to the fields of robotics, rehabilitation, costumer electronic devices, but also in the new field of soft robotics.

The technique used as transduction method allows to remove most of the stiff components that block the flexibility of the sensor, and to infer the internal structure of the domain under study by reconstructing its conductivity map. By applying the technique to a material that changes its resistivity according to applied forces, it is possible to identify these changes and then localise the area where the force was applied. We tested the system when applied to flat and curved surfaces.

In order to fully control all the parameters during the measurements we present a low-cost driving/measurement electronics and an inverse solver software able to perform similarly to the ones already developed in other researches. We then tested the system under different configuration and over different structure and scenarios. For all configurations, we evaluate the sensor's capabilities to detect forces applied over a single point, over multiple points, and changes in the underlying geometry. We also tested the system when applied to a natural soft deformable material such as the human skin. The results are all promising, and open the way for the application of such sensors in different robotic contexts where deformability is the key point.

The main contribution of the work is to introduce the Electrical Impedance Tomography to the field of deformable structure. This approach can be used in futuristic application such the ones involving the soft robotic filed where there are strong requirements on the deformability and adaptability of the technology used to develop these robotic devices.

# *Acknowledgements*

My greatest gratitude is for my supervisor Prof. Kenji Suzuki for giving me the opportunity to be part of his laboratory, for his valuable support, and guidance. He encouraged me to continue pursuing this work even when it seemed there was no hope in succeeding. The work done in this thesis could not have been accomplished without him.

My gratitude is also for Prof. Yoshiyuki Sankai, and Prof. Hiromi Mochiyama for their valuable supervision and inspiring comments on this work.

I would also like to thanks all the members of the Artificial Intelligence Laboratory for their friendship, and support. Thanks to make me feel home since the first day, and for sharing with me so many nice memories.

# Contents

# List of Figures

# List of Tables

# List of Abbreviations

|  |  |
|---|---|
| **AC** | **A**lternating **C**urrent |
| **DC** | **D**irect **C**urrent |
| **EIT** | **E**lectro **I**mpedance **T**omography |
| **EMI** | **E**lectro-**M**agneto **I**nterference |
| **FEM** | **F**inite **E**lement **M**ethod |
| **MWR** | **M**ethod of **W**eighted **R**esiduals |
| **PSF** | **P**oint **S**pread **F**unction |
| **SVD** | **S**ingular **V**alue **D**ecomposition |

# List of Symbols

| | |
|---|---|
| $A$ | Magnetic vector potential |
| $B$ | Magnetic filed |
| $D$ | Electric displacement |
| $E$ | Electric filed |
| $H$ | Magnetic filed |
| $I_i$ | Current |
| $J$ | Electric current density |
| $J_c$ | Conduction current |
| $J_s$ | Current sources |
| $\mathbf{J}_M$ | Jacobian Matrix |
| $K$ | Stiffness matrix |
| $M$ | Shape function |
| $N$ | Number of electrodes |
| $n$ | Normal vector |
| $R$ | Residual |
| $\mathbf{R}$ | Regularisation matrix |
| $S$ | Area of an element of the FEM mesh |
| $T$ | element of the FEM mesh |
| $t_i$ | $i^{th}$ time step |
| $V_i$ | Voltage potential |
| $W$ | Weighing function |
| | |
| $\Gamma$ | Boundary of the domain as $\partial\Omega$ |
| $\epsilon$ | Permittivity |
| $\mu$ | Permeability |
| $\xi$ | Coefficient of the weighting matrix |
| $\sigma$ | Conductivity of the medium |
| $\psi$ | Electric potential |
| $\psi_{fem}$ | Electric potential over all the elements of the FEM mesh |
| $\Omega$ | Surface or volume of the domain |
| $\partial\Omega$ | Boundary of the domain |
| $\omega$ | Frequency |

*This work is dedicated to my beloved Laura*
*who convinced me in pursuing this experience, and has*
*been a constant source of support and encouragement*
*during the challenges of graduate school and life.*
*Words cannot describe how lucky I am*
*to have her in my life.*

# Chapter 1

# Introduction

Robots and robotic devices are continuously improving and making fast steps in our life, by becoming more ubiquitous and present both in the workplace, and into other daily activities. As the integration progress is becoming more popular, additional precautions have to be taken into account in order to ensure safety for the humans and objects that surround the robot. The common approach that separate humans and robots using protective cages is no longer adequate, especially when future scenarios where a close collaboration between the robot and its human operator are considered. Consequentially, it is important to provide solutions that implement sensing capabilities to robots in order to collect information about the surroundings and thus plan save motion-paths that avoid static and moving objects and, in case of imminent collision, minimise the damages by performing avoidance manoeuvre or gently stop its action.

Beside safety, the interaction itself is another important aspect that should be taken into account. Tactile and haptic feedback from humans can be a useful additional and more direct channel of communication that can result in being a more natural and understandable interaction method. In fact, information provided by touch is important for humans since from those is possible to extract valuable data that can help to understand the meaning of the interaction itself. Having such capabilities will help in the development of the next generations of robots that will have smoother and softer surfaces to facilitate the interaction and collaboration not only with humans but also with other robots.

## 1.1   Tactile Sensing for Robots

The field of tactile sensing is very promising, for this reason in the last 30 years [1] many researchers focused their works on it. Particular interest has been placed on the problem of grasping control with robotic hands [2], but recently, with the growth of interest in humanoid and companion robots, the investigations on large scale robotic sensing is increased [3]. Nevertheless, tactile sensing is a very hard problem, and it involves several engineering issues that often require special processing equipment. In addition, there are fundamental technological difficulties that limit the direct transition

from the development of a single working sensor to a more complex network of sensors that is spread over large surfaces. However, different solutions that tackle and try to overcome the problem can be found in literature. These arrays of sensors, commonly referred as *artificial skins*, consist in a group of distributed sensors that are connected together in order to provide information over the sensing area. The sensor network is usually considered large (i.e. able to cover completely a wide portion of the robotic device) and able to conform over different 3D shapes —including curved and mobile parts— for witch it was design.

In order to replicate the capabilities of the human skin, a diversity of sensing principle has been adopted in the development of the single sensing elements composing an artificial skin [4]. These, used alone or in combination with others, allowed the development of artificial skins capable to distinguish between different phenomena, such as pressure, vibration, and temperature. Regarding tactile sensing, the main transduction methods identified so far belong to the following classes: resistive, capacitive, piezoelectric, magnetic, optical, and ultrasonic. Among these, capacitive sensing gained importance especially in the costumer electronics. The technology has excellent sensitivity, a good spatial resolution, and a large dynamic range. As drawbacks, capacitive sensors are very susceptible to noise —especially over large surfaces, suffer from stray capacitance, and the measurement system can become complicated as the size of the sensor grows. Similarly, resistive sensors (e.g. piezo-resistive, and strain gauges) are among the most used technology; the success is brought from the low cost, and the high spatial and temporal sensitivity. The weakness of the technique lie in the low repeatability rate, high hysteresis —especially for piezo-resistive sensors, and noise sensitivity. All of these can limit the application of resistive-based sensor. Ultrasonic sensing, i.e. using resonant property as a means to detect changes over the domain, has the major advance of using simple circuitry: a vibration speaker and a piezo-electric microphone. The technique provide developers with possibilities to flexibly design, and does not use conductive or magnetic components. This makes it safe for direct interaction and non susceptible to electromagnetic interference. However, even if used in combination with a material that conducts the vibration efficiently, vibration is dumped in function with the distance from the source. Thus, if the artificial skin is large, the sensitive area is limited to a small area between the speaker and microphone. Other limitations are related to the material, shape, and ambient noise. Optoelectronics are also a good candidate for pressure sensors. The technique allows the development of (semi-)transparent devices that are fast in response, have good sensing capabilities with good repeatability and reliability, and

are immune to electromagnetic field. But the need of smaller hardware architecture and low power consumption, make this technology difficult to be used. A comparison between the most common sensing techniques is presented in Table 1.1.

### 1.1.1   Problem Statement

An additional shared disadvantage among the presented transducing mechanism consists in the need of wires to connect the different sensing unit that are part of the network. The use of a large number of distributed wires not only forms an excellent antenna for electromagnetic noise, but also reduces the mobility of the robot by making it more bulky in order to contain all the components. This issue is especially crucial in the field of soft robotics [16, 17] where robots not only move more naturally, by mimicking biological systems, but are also made of material (e.g. silicon rubber) that can deform and easily adapt to different situations. These novel technologies have more demands than more traditional robotic platforms since it is fundamental to maintain their *soft* properties in order to be advantageous. The use of this paradigm will open a new path for the development of novel robotic system that are intrinsically compliant and safer in case of accidental collision of the robot with a human. Sensors, or artificial skins, for this type of robots should be flexible, and able to follow the changes undergoing in the robot structure while maintaining the sensing capabilities even under large deformations.

Among the various approaches that can be used in such context, the one we found the most promising, is the use of a tomographic technique known as Electrical Impedance Tomography (EIT). In this technique, a small current is injected into a conductive domain, and voltage potentials are then measured around the boundaries in order to infer the internal structure of the domain. Approaches that use this technique are not new and they have been used in different application domain spanning from the geophysical inspection [18, 19] to biomedical measurements [20, 21], and recently robotic applications [22, 23]. In all of those applications, the Electrical Impedance Tomography has been used to localise areas of inhomogeneity within the domain caused by the presence of elements that change the domain conductivity. If applied to a stretchable conductive substrate, as in [24–27], the technique can be used to develop a flexible sensor with arbitrary size and shape, that do not suffers from the presence of wires within the sensing area. Even if it sounds promising, the technique has some drawbacks, especially related to spatial resolution.

| Type | Method | Pros | Cons |
|------|--------|------|------|
| Capacitive [5, 6] | Change in capacitance | Excellent sensitivity, good spatial resolution, large dynamic range | Stray capacitance, susceptible noise, complexity in the electronics |
| Piezoresistive [7, 8] | Change in resistance | Very good spatial resolution, and high scanning rate | Hysteresis, lower repeatability, high power consumption |
| Optoelectric [9, 10] | Light intensity change | Good sensing range and reliability, hight repeatability and spatial resolution, immune to EMI | Non-conformable, buky in size |
| Strain Gauges [11, 12] | Change in resistance | Good sensing range, low cost | Susceptible to temperature changes and humidity, EMI can induce errors, non-linearity in measurements |
| Combination of sensors [13–15] | Complong of multiple intrinsic parameters | Can overcome limitation by using combination of measurements | Higher assembly cost |

TABLE 1.1: Comparison between conventional sensing methods.

## 1.2   Purpose of This Research

By exploiting this sensing technique, the aim of this dissertation is to investigate and present a low-cost wearable sensor that is able to adapt to different surfaces and still provide information even when deformed. As discussed earlier, out main intent is developing a system able to detect and monitor pressure changes that are applied over the surface of the surface where the sensor is applied. In order to achieve such goal, it is needed to develop a system that consists in the following components

- A driving/measurement system used to acquire data

- An image reconstruction software

- A conductive domain used for sensing

Due to the nature of the problem involved in the use of EIT as sensing method, the hardware used in the measurements plays a crucial role, as well in the techniques used in the image reconstruction. For this reason, all of these have to be verified by using experimental validation. The system described in this thesis is the results of various attempt in hardware development. However, only the last version, the one used in all the experiment will be discussed in details.

In term of reconstruction software, there are different challenges involved in developing a functional EIT system that can fit the purpose of this thesis. In order to accomplish this, an appropriate and in-depth knowledge of the mathematical bases involved in the image reconstruction, together with programming capabilities are essential.

Regarding the developed conductive sensor, several different design and prototypes have been carried out involving the use of different conductive materials shaped in different form to which a fixed number of electrodes (eight) have been attached. However, in this thesis only the results related to a singular shape—circular—applied over different geometries and materials will be presented. In addition, a natural conductive material has been used to test the extendability of the system to different situations.

Our main contribution is, starting from the current solutions, the development of a simpler and similar effective sensor that can be used in novel research areas where simplicity and deformability are the key points. The sensor we developed is small in size, so the circuitry and the cable assemble that compose the whole electronics do not interfere in the morphological changes of the device where it is embedded, and modular in order to adapt to different situations. As this thesis will show, an in deep study on the mathematical background of EIT has been carried out in order to fully exploit its properties for the applications presented in this thesis. Additionally, the

results presented open novel research paths, and provide solutions to current problems in different aspect of the robotic field.

## 1.3   Thesis Outline

The research presented in this thesis is organised i different chapters. Chapter 2 introduces the related work in the field of EIT and shows the limitations of the technique. Chapter 3 presents the main core of this thesis by providing the basis of the imaging reconstruction algorithms, together with details about the mathematical model used to solve an EIT problem. The measurement system, which consists in a driving and readout electronics, and a MATLAB® based control software, will be presented and discussed in Chapter 4. Chapter 5 will introduce a series of preliminary experiments used to characterise the conductive domain used in later applications . These, are introduced and discussed in Chapter 6. Finally, a general discussion on the results is presented in Chapter 7 followed by conclusions and a consideration about future work that are presented in Chapter 8.

Parts of the thesis have been already published or are in the process of being submitted for publishing. The background information about EIT in Chapters 3 and 4, along with preliminary results related to the development of the fabric-based sensor in Chapter 5, have been published in a conference paper and then extended into one journal. Part of the results published in Chapter 6 have been published as conference paper, while the remaining are in the process of publication.

# Chapter 2

# Related Works

The tomographic technique known as Electrical impedance tomography (EIT) allows to generates maps of electrical conductivity over a domain under study by injecting electrical current and measuring electrical potentials. The domain can be either two– or three-dimensional. In this thesis, EIT is applied over a conductive fabric and used to monitor pressure changes when the system is applied over different geometries and materials. The use of such technique in the presented combination, can applied in the development of a wearable system that can detect contact forces and displacement of the underlying structure. The main advantage of this technique consist in the fact that the sensitive are does not contain any wire from the measurement system since they are all placed around the boundaries.

## 2.1 Background of EIT

From a historical prospective, EIT EIT is a relatively young but mature technique, which has been used in different disciplines and applications since its early ages [28]. In fact, thanks to its unique portability, and low cost has attracted physicists interested in applying it to bio-impedance measurements, thanks to its safety it has been used engineers and clinicians that applied it to overcome specific limitation of other techniques, and as a consequence of its ill-posed nature, mathematicians interested in finding uniqueness profs to inverse problems.

EIT is an imaging technique which is used to determine physical parameters within a region of interest by using a non-invasive approach. Other similar techniques are Magnetic Resonance Imaging (MRI), X-Ray Computed Tomography (CT), Positron Emission Tomography (PET), and ultrasound. All of these have advantages and disadvantages when applied to specific case, a comparative review is out of the scope of this dissertation and the reader is invited to refer to [29] for a comprehensive discussion.

EIT started to be used as alternative tomographic technique for traditional imaging by overcoming the disadvantages of these technique in being expensive, and in providing a biological hazard to the patient and to the technician while in use. The first attempt of EIT

imaging has been done by assuming that current *flows in a straight line* as in the beans of a X-Ray CT scanner [30]. The method was successful, but had very low resolution and was prone to artefacts. Since the initial attempts, a series of different image reconstruction techniques have been investigated and developed. The first real successful method was reported in [31] in which the initial idea has been applied to a single-frequency system used to scan part of a human body (in vitro). After the first prototypes, different new model were developed that were able to extract more properties from the analysed domain by the use of a multi-frequency approach. The initial success, and the following systems created a new interest in the clinical field that in the following years, new developments were made and the technique was applied in more than ten different area including imaging for breast cancer and brain function.

When EIT is compared to other techniques, it suffers from some limitation that may preclude its adoption for typical application in medical diagnosis. Among the main limitations there are its low spatial resolution, susceptibility to noise and and electrode errors, and large variability between subjects that prevent its use for anatomical imaging. However, EIT as proven to be worthwhile as diagnostic tool for medical clinicians. In fact, among the advantages there is a low cost in the instrumentations, and small in size—compared to others such as MRI and CT—that makes it more suitable to be used in different situation. Furthermore, EIT does not use any ionising radiation and thus make it safe to be used both for the patient involved i the measurements and the technician that uses the system. So far we introduced only applications related to the medical field, but since its early ages its use has also be considered in other fields, and especially in the industrial one. In industrial application, EIT is mostly used to determine the composition and structural information of materials in well defined region of interest, online monitoring and process control by applying the same procedure used in the clinical-based cases. In the following sections, we will introduce and discussed applications where EIT is commonly used.

## 2.2 Common EIT Applications

Electrical Impedance Tomography has been used mostly in the following field: i) industrial, ii) geophysical, and iii) medical . In *industrial* applications, EIT has been used to monitor fluids and its behaviour in pipelines, mixing vessels, and in non-destructive testing in order to test the structural integrity of materials or buildings [32–34]. EIT has been also largely used in *geophisical* applications that incluse geophysical prospecting, cross borehole measurement and surface measurement [18, 19, 35]. However, the technique has mostly

being used in *medical* applications for all sorts of monitoring purposes. In the specific it has been used to monitor function of lungs—thorax functional imaging—and hearth, to visualise brain functions, to measure gastric imaging, to identify and and to classify tumours in breast or brain tissue [36–41].

### 2.2.1 Application in Industrial Process

In Industrial applications, EIT is used to provide information of conductive fluids (e.g. water) that fill basins, or flow within vessels or pipes. In addition to EIT capacitance tomography is also used for these applications [42]. The techniques can be used to monitor industrial process, determine the presence of inhomogeneities in chemical reactions and their spatial-temporal concentration variation. These are also used to measure the mass of liquid moved during each phase of the industrial processes, or to identify sections where there are impediments or leakages. Example of application in this field are presented and discussed in [43, 44].

### 2.2.2 Application in the Geophysical Field

EIT, in geophysical application, is typically used to obtain core sample data, to probe the soil in order to detect the presence of minerals close to the earth's surface, and to perform scanning of borehole. One of the main use of the technique in this field is to retrieve information of the inner structures of geological objects. In fact, rocks are resistive and this value can change considerably the order of magnitude with the change of the type of rock, its composition, structure, and amount of water it contains. In order to obtain these information, an array of electrodes is placed in the ground and the soil conductivity is returned by applying inverse solving of the classical EIT problem. The distance between electrodes—usually equally spaced—changes the spatial resolution and the depth of the measurement.

### 2.2.3 Medical Application

EIT found its main application in the medical field since its early age. Now it is an established technique to sample and recognise biological tissues by using the information such as conductivity and permittivity [45] which change according to tissue's state of health, and during the normal functioning of the organ. The property is been studied and now, it allowed the development of different technique used to discriminate the presence of tumours within organs as presented in Jessinet [46] and in Surowiec et al. in [47]. EIT has also been used in other medical applications, in which the measure

of the bio-impedance is used to evaluate the global states of biological systems—e.g. measure the function of the cardiac and respiratory apparatus, to quantify the tissue composition, or measure the amount of fluid within the body. Bio-impedance measurements can be taken in order to obtain more detail and thus evaluate the tissue under study. This technique is applied locally and often used to detect the presence of tumours in the mammary glands and in the subcutaneous tissue. The techniques been used also to obtain three-dimensional information and thus provide a comprehensive physiological model of the section of the body under study. In order to do so, one or more two-dimensional slices are acquired through the patient, and the obtained images can be interpolated in order to infer what is contained between them.

## 2.3   EIT as Wearable Technology

While in the field just introduced there is a trent to expand current EIT applications to three-dimensional imaging, this thesis in mainly focused on two-dimensional ones where EIT is used to monitor changes that occur on a conductive surface. The combination of a conductive textile and the use of EIT enable the development of artificial skins that can overcome current limitations of conventional point based sensor mapping such as the implementation of touch sensitive application over complex geometries, or deformable bodies. In addition the previously introduced applications, EIT has been used also as a transducing method for pressure mapping but still its use is relatively new in the research field. In fact, nowadays, classical sensing techniques—based on resistive or capacitive changes—are still widely studied. The main reason lies in the fact that EIT has a poor spatial resolution, but the advantages brought by a large sensing area and its deformability make the technique suitable for many applications.

### 2.3.1   Pressure Monitoring and Mapping

Fulton and Fulton et al. in [48] introduced the idea of using EIT to develop a pressure sensor. Even though the technology was ready, the experimental trials failed in the identification of a suitable material to be used as conductive substrate. The idea was then reconsidered years later in [49] where the described developments have shown promising results especially in the adaptability and flexibility of the method to different geometries (stiff underlying structure), and the integration of these sensors in robotic applications as artificial skins.

## 2.3.2 Robotic Skin Application

Human-robot interfaces have been widely developed in the last years. Despite this, researchers are still looking for a good solution to be used in the development of these interfaces. Traditional matrix base approaches can be used in many applications and can easily adapt to many surfaced. However, when it is required to cover complex geometries, this method suffers from limitations in their implementation. With the use of different conductive materials, and an appropriate sensing method, it is possible to overcome such limitation and thus implement deformation and pressure sensing ability even in the case of complex geometries such as the robot face or hand. EIT-based sensing has been already used to develop such sensors [24–27, 50] since its lack of rigid components in the sensing area enable it to easily conform to the underlying geometry. In addition, by properly tuning the system, it is possible to detect multi-touch stimuli while maintaining the sensor's deformation sensing ability.

# Chapter 3

# Methodology

EIT is an imaging technique that allows to infer the internal structural of a body by solving an inverse problem that use as starting point the measurements taken at the boundary of the domain under study. In this chapter, we will introduce the image reconstruction algorithm, and we will provide an overview of the mathematical fundaments used to model the EIT problem and the mechanisms used for the image reconstruction.

## 3.1   Image Reconstruction Algorithm

In order to solve the EIT problem, different algorithm have been introduced and developed. These can be organised in four main classes, each of these are based on different acquisition methodology. The classes can be described as follows.

*Time difference imaging* is a technique that is used to reconstruct images that represent variation of impedance over a non-fixed time interval. The main idea consists in acquiring a series of potential measurements $V_i$ at time $t_i$, and a second set $V_{i+n}$ at time $t_{i+n}$, where $n$ is a non-fixed time interval. The algorithm then computes the differences in the conductivity between the two time frames. The method is widely used to monitor temporal phenomena especially in medical application, e.g. monitoring patient ventilation. Among the main advantages of the method there is its ability to improve the stability of the reconstructed image when an unknown contact impedance has been used in the model, and when an erroneous or non precise positioning of the electrodes, poor information about the boundary shape. In addition, the method allows to approximate three-dimensional electrical fields as a composition of multiple two-dimensional measurements [51, 52]. The change in conductivity can not be computed directly since EIT is a non-linear problem. For this reason, it can be computed by applying a series of non-linear iterative algorithms.

A second class of reconstruction algorithm is the one known as *absolute* or *static imaging*. Here, the images are reconstructed computing the absolute impedance distribution on the domain by using

an iterative approach. This method is extremely sensitive to uncertainty in electrode position, and it is generally slow, since at every step of the iteration, the mathematical model has to be updated with the newly acquired measured data.

As previously discussed, some EIT system are able to perform scanning using difference frequency. *Multi-frequency* imaging can produce images for frequency-dependant changes in the impedance. The comparison is similar to the one applied in the *time difference imaging*, or by injecting current at different frequency.

Last class of algorithm is known as *dynamic imaging*. The technique is mostly used where fast conductivity changes are involved. The working principle si similar to the one used in *time difference imaging*, but the time interval is much faster.

### 3.1.1  Forward Problem

Working with an EIT problem involves to calculate and solve a forward problem and an associated inverse problem. Here, the forward problem is used to model the measuring process, while the inverse one is used to retrieve the conductivity distribution starting with the measured data. The starting point of all the process are the Maxwell's equation of electromagnetism [53], that under the assumption of using low frequency can be traced back to a Laplace equation with complex values. In this section we are going to derive these equation for the 2D case.

The initial step is deriving the equation to construct a physical model and then solve the forward EIT problem. The equations link the measured voltages, injected currents, and a conductivity distribution and are used to compute boundary potentials starting from the given electrical conductivity (or permittivity) distribution. If a non-homogeneous medium is considered, Maxwell's equations can be written as:

$$\nabla \times E = -\frac{\partial B}{\partial t} \tag{3.1}$$

$$\nabla \times H = J + \frac{\partial D}{\partial t}, \tag{3.2}$$

where $E$ is electric field, $H$ is magnetic field, $B$ is magnetic induction, $D$ is electric displacement, and $J$ is electric current density.

If the injected currents are time-harmonic with frequency $\omega$, the electric and magnetic fields can be written in the form:

$$E = E e^{j\omega t} \tag{3.3}$$

$$B = B e^{j\omega t}. \tag{3.4}$$

If the medium is isotropic, the following relations are valid:

$$D = \epsilon E \tag{3.5}$$
$$B = \mu H \tag{3.6}$$
$$J = \sigma E, \tag{3.7}$$

where $\epsilon$ is the permittivity, $\mu$ is the permeability, and $\sigma$ is the conductivity of the element. Usually, to simplify the computation, EIT bodies are approximated as isotropic. As a consequence, Equations (3.5–3.7) can be used to rewrite Equations (3.1) and (3.2) by assuming that the injected current is time-harmonic.

$$\nabla \times E = -j\omega\mu H \tag{3.8}$$
$$\nabla \times H = J + j\omega\mu\epsilon E. \tag{3.9}$$

Current sources in EIT are usually denoted with the symbol $J_s$. The current density can then be rewritten as $J = J_c + J_s$, where $J_c = \sigma E$ is the conduction current. It is possible to rewrite Equations (3.8) and (3.9) with this notation:

$$\nabla \times E = -j\omega\mu H \tag{3.10}$$
$$\nabla \times H = J_s + (\sigma + j\omega\epsilon)E. \tag{3.11}$$

The equations just presented are the full Maxwell's equations. From these, in most of the EIT application some assumptions are made. The first one consists in considering static conditions. This means that

$$E = -\nabla\psi - \frac{\partial A}{\partial t}, \tag{3.12}$$

where electric potential is $\psi$, and the magnetic potential vector $A$ can be neglected since the frequency is low. As a consequence, it is also possible to neglect the effect of the magnetic induction that causes the induced electric field. This is possible if:

$$\omega\psi\sigma L_c \left(1 + \frac{\omega\epsilon}{\sigma}\right) \ll 1, \tag{3.13}$$

where $L_c$ is a distance over which E varies significantly. Since it is very small, it is possible to neglect the effect of the magnetic field.

A second simplification that is made consists in neglecting the capacitive effects ($j\omega\epsilon E$ in Equation (3.9) ). This is valid when:

$$\frac{\omega\epsilon}{\sigma} \ll 1. \tag{3.14}$$

By considering all these approximations, the Maxwell's equations assume a linear form, and when applied to an isotropic medium under quasi-static conditions can be rewritten in the form:

$$E = -\nabla\psi \tag{3.15}$$

$$\nabla \times H = J_s + \sigma E. \tag{3.16}$$

By applying the divergence theorem on both sides of Equation (3.16) and substituting Equation (3.15) into (3.16) it becomes:

$$\nabla \cdot (\sigma\nabla\psi) = 0, \tag{3.17}$$

which can be considered true since no further current sources ($J_s = 0$) are acting inside the body, only the one that is applied at its boundary.

The conductivity $\sigma$, and potential $\psi$, since they can vary over the object, can be expresses in their functional form as $\sigma(x)$ and $\psi(x)$, where the variable $x$ represents any point considered in the volume (three-dimensional case) or over the surface (two-dimensional case) of the domain under study. By using such representation, Equation (3.17) can then be written as:

$$\nabla \cdot (\sigma(x)\nabla\psi(x)) = 0, \tag{3.18}$$

To complete the model it is needed to model the electrodes attached at the boundary of the studied domain. The complete electrode model [54] considers both the contact impedance between the electrode and the body, and the shunting effect of the electrode itself. The model is expressed by Equation (3.18), together with the following conditions at the boundary [55]:

$$\psi(x) + z_i\sigma\frac{\partial\psi(x)}{\partial\mathbf{n}} = V_i \ \ x \in e_i, \ \ i = 1, 2, \ldots, N \tag{3.19}$$

$$\sigma\frac{\partial u}{\partial\mathbf{n}} = 0 \ \ \text{in the gap between electrodes.} \tag{3.20}$$

$$\int_{e_i} \sigma\frac{\partial u}{\partial\mathbf{n}} ds = I_i \ \ \text{on} \ e_i, \ \ i = 1, 2, \ldots, N. \tag{3.21}$$

The model considers the existence of a discrete number of electrodes $e_l$ of finite size, the shunting effect of a conductive electrode, and the potential drop due to the electrode's contact impedance $z_i$.

In addition it requires that the current density over the electrode surface $s$ is equal to the current $I_i$. In the equation $\mathbf{n}$ is the normal vector to the electrode surface, while N is the total number of electrodes used.

To ensure the uniqueness of the solution the conservation of charge theorem must also hold

$$\sum_{i=1}^{N} I_i = 0, \tag{3.22}$$

together with a choice of a ground or reference voltage

$$\sum_{i=1}^{N} V_i = 0. \tag{3.23}$$

### 3.1.2   Finite Element Method

The Finite Element Method (FEM) is a numerical technique used to find approximate solutions to boundary value problems for partial differential equations. The method was originally developed as a tool for design, however, now it is a common tool for numerous fields and it has been applied to a wide variety of engineering problems. It has been also used to model electromagnetic and electrostatic fields [55]. The method, thanks to its adaptability and the ability to be applied to any arbitrary geometry and to various boundary condition, is the most common approach used to provide numerical solutions of EIT problems [31]. The rest of the section is based on the work of Chiari et al. [56].

If we consider a continuum problem of any dimension, the dependent variables (also known as field variable) of interest, e.g. the electric potentials in an EIT problem are defined over a infinite number of variables since the domain consists in an infinite number of points. By applying the finite element method, the problem is first discretised into a finite number of elements that form a finite element mesh (Figure 3.1). In each of these elements the variable of interest is no more dependent to infinite point, but it is approximated by functions that are defined only within the single element of the mesh. The interpolation functions are predetermined, known functions of the independent variables; and these functions describe the variation of the field variable within the finite element. A node is a specific point in the finite element at which the value of the field variable is to be explicitly calculated. In the finite element approach, the nodal values of the field variable are treated as unknown constants that are to be determined. The interpolation functions are most often polynomial forms of the independent variables, derived to satisfy
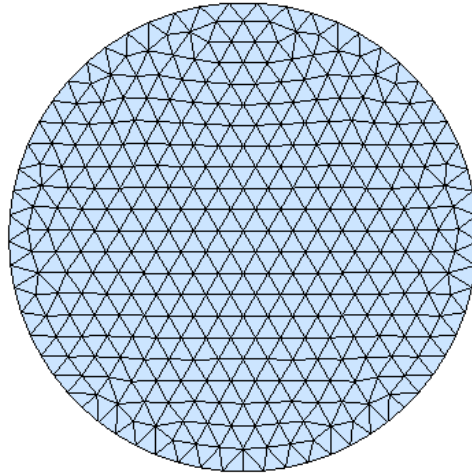
FIGURE 3.1: A 2D circular mesh generated applying
the Finite Element Method. The mesh has 661 triangles
and 362 nodes.

certain required conditions at the nodes. Although it is possible to
use higher order shape functions, most of the EIT works use linear
shape functions, and all the elements are connected.

Usual approached to formulate Finite Element problems can be
grouped into three main approaches [56]; i) *direct*, ii) *variational*, and
iii) using the method of *weighted residuals* (MWR). Although the *direct*
approach is limited in its application, it is the most intuitive way to
explain how the FEM works. A different method is the one based on
the *variational* approach. The method relies on the calculus of varia-
tions and deals with maximising or minimising functionals. The ap-
proach is used to extend the FEM to a class of problems that can not
be approached by the classical direct approach. Among these, prob-
lem involving non-constant conductivity over time or space, when
interpolation functions are not linear, or when the finite element mesh
is made of simplex that are neither triangles nor tetrahedrons. The
last method that can be used to solve a FEM problem is known as
*method of weighted residuals*, among the three it is the most versatile
approach. The starting point is the governing equations of the prob-
lem and does not rely on a variational statement. The method is
widely used and it is very beneficial for the class of problems where
no functional is available. Main applications where it is used are the
non-structural ones such as heat transfer and fluid mechanics.

The solution of a continuum problem, approximated by the FEM
can be outlined regardless of the particular finite element method
used as follows:

   1. Convert from continuum to discrete. The main function of the

FEM method consists in subdividing the domain into a discretised number of elements connected by nodes. These elements are, n general, non-uniform, and non overlapping. Common simplex for the two-dimensional case are triangles and rectangles, while tetrahedral and hexahedral elements are mostly used in the three-dimensional case. In this work, since the domain under study is two-dimensional, only triangular simplexes are used.

2. Definition of the shape functions. The field variable, as previously introduced, is approximated by functions that are null over all the domain except on each single element of the mesh. Even if a common approach consists in the use of polynomial functions to solve FEM problem, in this work we mostly used linear interpolation

   Despite the fact that polynomial functions are mostly used to solve FEM problem, in this work we mostly used linear interpolation.

3. Compute the elements' values by solving the local matrix for each simplex.

4. Combine the properties of each element in order to obtain a system of equations of local matrices.

5. Impose the boundary conditions to the mesh. These conditions can act at different level of the mesh. In detail, they can prescribe a specific value to the field value of an element (Type I, Dirichlet condition), they can impose a specific value to the derivative of field value of an element (Type II, Neumann condition), or be a combination of both (Type III condition).

6. Solve the system of equations by considering all the constraints imposed by the boundary conditions.

7. In case of iterative or adaptive algorithms, perform additional computations.

By applying the FEM to the problem, it is converted from its continuum form into a discretised one. This discretisation is usually in the shape of triangular elements arranged into a finite element mesh (Figure 3.1). When solving an EIT problem, it is a common approach to assume constant the conductivity distribution of each of the elements in the mesh, and to assume linear the voltage distribution over the domain. In figure 3.2, an individual element of the mesh is shown. For the two-dimensional case, each element is a triangle in which its are named as $1(x_1, y_1)$, $2(x_2, y_2)$, and $3(x_3, y_3)$ with corresponding function $N_1$, $N_2$, and $N_2$, and nodal potential $\psi_1$, $\psi_2$, and $\psi_3$.
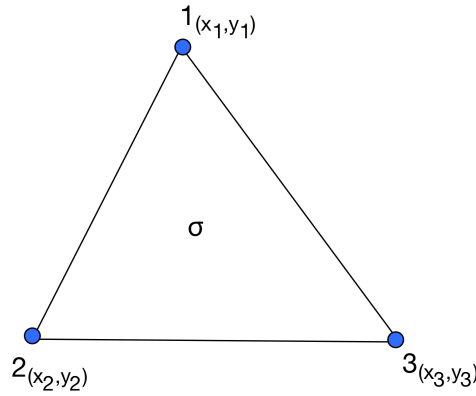
FIGURE 3.2: An individual element from the Finite Element mesh.

### 3.1.3   Linear Interpolation Functions

Following the approach used in [57], in this section we are going to introduce and derive the linear interpolation functions used in this work. These have been applied to the method of weighted residuals in order to solve the EIT problem. Since it considered is two-dimensional, the following equations are derived by considering simplex in the form of triangle over which the potentials vary linearly within all the elements. As a consequence, the potentials at each node can be written as:

$$\psi(x,y) = p + qx + ry = [1\ \ x\ \ y][p\ \ q\ \ r]^T, \qquad (3.24)$$

where $p$, $q$, and $r$ are the coefficients of the linear combination. Using (3.24) and applying to each of the node of the triangle, it becomes:

$$\psi_1(x_1, y_1) = p + qx_1 + ry_1 \qquad (3.25)$$
$$\psi_2(x_2, y_2) = p + qx_2 + ry_2 \qquad (3.26)$$
$$\psi_3(x_3, y_3) = p + qx_3 + ry_3. \qquad (3.27)$$

It is possible to combine these equation into a single system that can be written as:

$$\psi(x,y) = \frac{1}{S} \left( \begin{bmatrix} \psi_1 & x_1 & y_1 \\ \psi_2 & x_3 & y_2 \\ \psi_3 & x_3 & y_3 \end{bmatrix} + \begin{bmatrix} 1 & \psi_1 & y_1 \\ 1 & \psi_2 & y_2 \\ 1 & \psi_3 & y_3 \end{bmatrix} x + \begin{bmatrix} 1 & x_1 & \psi_1 \\ 1 & x_2 & \psi_2 \\ 1 & x_3 & \psi_3 \end{bmatrix} y \right)$$

(3.28)

Where, $S$ is twice the area of the element $T$, $S = 2 \begin{bmatrix} 1 & x_1 & y_1 \\ 1 & x_3 & y_2 \\ 1 & x_3 & y_3 \end{bmatrix}$.

By expanding (3.28) and then re-combining it as a summation, it becomes a linear combination with coefficient $\alpha$, $\beta$, and $\gamma$:

$$\psi(x,y) = \sum_{i=1}^{3} \frac{1}{S}(\alpha_i + \beta_i x + \gamma_i y)\psi_i.$$

(3.29)

Consequently, it is possible to express the approximation of the potential within any element of the two-dimensional mesh as:

$$\psi(x,y) = \sum_{i=1}^{3} M_i \psi_i,$$

(3.30)

where $M_i$ the shape function (i.e. interpolation function) that can be expressed as:

$$M_i = \frac{1}{S}(\alpha_i + \beta_i x + \gamma_i y) = \frac{1}{2T}(\alpha_i + \beta_i x + \gamma_i y)$$

(3.31)

By applying the function at each of the three nodes of the triangle leads to:

$$M_1 = \frac{1}{2T}\left((x_2 y_2 - y_2 x_3) + (y_2 - y_3)x + (x_3 - x_2)y\right)$$

(3.32)

$$M_2 = \frac{1}{2T}\left((x_3 y_1 - y_1 x_3) + (y_3 - y_1)x + (x_1 - x_3)y\right)$$

(3.33)

$$M_3 = \frac{1}{2T}\left((x_1 y_2 - y_1 x_1) + (y_1 - y_2)x + (x_2 - x_1)y\right)$$

(3.34)

These functions are used to interpolate the value of the element between the vertices of the triangle. The functions $M_i$ are one at the corresponding vertex, while at the others take null value. The potential within a triangular element is fully defined, as expressed in Equation (3.30), by a function of the values of the potential at its three nodes.

### 3.1.4   Application to the MWR

Ordinary differential equation can be solved using the weighted residual method, in particular using Galerkin method. This is the most common method of calculating the global stiffness matrix in the finite element method. The approach can be used to solve Equation (3.24), starting with the following rewriting rewriting:

$$\nabla \cdot \sigma \nabla \psi_{fem} = R, \tag{3.35}$$

where the term $R$ is the *residual* matrix. In order to solve the problem, the value of $R$ in the equation should be zero, thus:

$$\int_{\Omega} WR \ d\Omega = 0, \tag{3.36}$$

where $W$ is the weighting function which is defined as:

$$W(x) = \sum_{i=1}^{n} \xi_i M_i(x), \tag{3.37}$$

where $\xi_i$ are the coefficients used to weight the shape functions $M_i$. By combining Equations (3.35) and (3.36),

$$\int_{\Omega} W \nabla \cdot \sigma \nabla \psi_{fem} \ d\Omega = 0. \tag{3.38}$$

Given a generic scalar function $f$, and given a generic vector function $v$, Equation (3.38) yields:

$$\int_{\Omega} \nabla \cdot (W \sigma \nabla \psi_{fem}) \ d\Omega = \int_{\Omega} (\sigma \nabla \psi_{fem} \cdot \nabla W) \ d\Omega \tag{3.39}$$

Boundary condition can be added to the previous equation by applying the Gauss Theorem to it:

$$\int_{\Omega} W \sigma \nabla \psi_{fem} \cdot \hat{n} d\Gamma = \int_{\Omega} (\sigma \nabla \psi_{fem} \cdot \nabla W) \ d\Omega, \tag{3.40}$$

where, $\nabla \psi_{fem} \cdot \hat{n} = \frac{\partial \psi}{\partial n}$, and $\Gamma = \partial \Omega$ represents the boundary. Therefore Equation (3.39) can be rewritten as:

$$\int_{\Omega} \sigma \nabla \psi_{fem} \cdot \nabla W \ d\Omega = \int_{\Omega} W \sigma \frac{\partial \psi}{\partial n} d\Gamma. \tag{3.41}$$

The just presented equation define the boundary integral over the whole mesh. On the contrary, when it is considered for a single element ,$i$, of the mesh the left hand side of Equation (3.41) changes and it is given by;

$$\int_{e_i} \sigma_i \nabla \psi_i \cdot \nabla W \ d\Omega \qquad (3.42)$$

By considering the FEM domain and using the presented Equations, yields:

$$\int_{e_i} \sigma_i \nabla \psi_i \cdot \nabla W \ d\Omega = \sigma_i \sum_{j=1}^{3} \phi_j \sum_{l=1}^{3} \xi_l K_{jl}^i, \qquad (3.43)$$

where $K_{jl}^i$ is the *local stiffness matrix* and can expressed as follows:

$$K_{jl}^i = \int_{e_i} \nabla M_j \cdot \nabla M_l \ d\Omega. \qquad (3.44)$$

By applying the FEM, for each element $T$ of the mesh we obtain a 3 x 3 matrix. This matrix (known also as local stiffness matrix) is used to link together the different element when propagating the forward solution.

### 3.1.5 The Jacobian Matrix

In some EIT applications it is often needed, and more convenient to solve the problem by computing the derivative of the voltage measurements with respect to the domain conductivity. These information can be expressed as a matrix that contains such information is the Jacobian Matrix [58] (or sensitivity matrix) and it can be denoted with the symbol $\mathbf{J}_M$. It generalises the gradient of a scalar-valued function of multiple variables, which itself generalises the derivative of a scalar-valued function of a single variable. The matrix has a size equal to the number of measurements times the number of the elements in the FEM mesh.

In this work, *dynamic imaging* has been used. As a consequence, to reconstruct the conductivity changes within the studied domain it is just needed to acquire two sets of measurements at different time intervals. The measurements are collections of voltage readings acquired as difference between electrode pairs. The first set, taken at time $t_1$t, is typically taken when any force or deformation is acting over the domain, and thus is used as reference. The laters, taken at time $t_i$ with $i = 2, 3, \ldots, \infty$, may contain alteration in conductivity or deformation of the domain.

By computing the difference between the two set of measured voltage we obtain $\Delta V$. With this value it is possible to obtain the variation in conductivity for each of the elements of the FEM mesh as a consequence of the change in the electric potentials in the time interval $\Delta t$. The following equation represents the relationship between thee element in the EIT inverse problem. Having this representation of the problem helps in simplifying its resolution since only few parameters have to be considered in its computation.

$$\Delta V = \mathbf{J}_M \Delta \sigma + \text{Noise}. \tag{3.45}$$

## 3.2 Inverse Problem

### 3.2.1 Singular Value Decomposition

In linear algebra, the Singular Value Decomposition (SVD) is a factorisation of a real or complex matrix. Since the decomposition does not require any special property (such as being symmetric, or having full rank) of the matrix to which it is applied, the method is very promising when used to solve the EIT inverse problem.

Lets consider $\mathcal{A} \in \mathbb{R}^{mxn}$ a rectangular matrix in which $m \leq n$. Then, the Singular Value Decomposition of $\mathcal{A}$ can be expressed in the form:

$$\mathcal{A} = USV^T = \sum_{i=1}^{n} u_i s_i v_i^T, \tag{3.46}$$

where $U = (u_1, u_2, \ldots, u_n)$ and $V = (v_1, v_2, \ldots, v_n)$ are matrices with orthonormal columns, $U^T U = V^T V = I$, and $S = diag(s_1, \ldots, s_n)$. The elements in $S$ are known as *singular value*, these are non-negative, and arranged in non-increasing order such that $s_1 \geq \ldots \geq s_n \geq 0$ by convention. The other elements, $u_i$ and $v_i$ are respectively the right and left singular vector of $\mathcal{A}$.

If $rank(\mathcal{A}) = k < n$, then the singular vectors $v_{k+1}, \ldots, v_n$ form an orthonormal basis for $null(\mathcal{A})$, while $u_1, \ldots, u_k$ form a basis for $range(\mathcal{A})$. On the contrary, if $rank(\mathcal{A}) < m$, then $v_1, \ldots, v_k$ form a basis for $range(\mathcal{A}^*)$, and $u_{k+1}, \ldots, u_n$ form an orthonormal basis for $null(\mathcal{A}^*)$. Here $\mathcal{A}^*$ indicates the conjugate transpose of the matrix $\mathcal{A}$.

In summary:

$$\mathcal{A}v_i = s_i u_i \quad i \le min(m,n) \tag{3.47}$$

$$\mathcal{A}^* u_i = s_i v_i \quad i \le min(m,n) \tag{3.48}$$

$$\mathcal{A}v_i = 0 \quad rank(\mathcal{A}) < i \le n \tag{3.49}$$

$$\mathcal{A}^* u_i = 0 \quad rank(\mathcal{A}) < i \le m \tag{3.50}$$

$$u_i^* u_j = v_i^* v_j \tag{3.51}$$

$$s_1 \ge s_2 \ge \ldots \ge s_n \ge 0 \tag{3.52}$$

In order to understand the well– or ill–conditioning of the problem it is possible to analyse the condition number of the matrix. This value measures how much the output value of the function can change for a small change in the input argument. It is also used to measure how sensitive a function is to changes or error input, and the precision level of the computations. For a matrix $\mathcal{A}$ the condition number can be computes as the ration $s_1/s_n$. Generally, if the problem has a low condition number it i said to be well-conditioned, on the contrary if the condition number is hight the problem is said to be ill-conditioned.

### 3.2.2 Tikhonov Regularisation

Usually, inverse problem are ill-conditioned systems. For this reason it is needed to introduce a regularisation method that reduce the effects of numerical errors by smoothing the data and restoring continuity of the solution [59]. Conventional regularisation methods include Tikhonov regularisation and approaches based on singular value decomposition (SVD) [53]. Although SVD, as we discussed earlier, can be used as a tool to study the ill-conditioning of matrices, a commonly more accepted method is the use of Tikhonov regularisation that is a more efficient and simpler than SVD.

Tikhonov regularisation works by minimising the least-square function. Thus, Equation (3.45) can be written by using this approach as:

$$\min_{\Delta\sigma}\{||\mathbf{J}_M\Delta\sigma - \Delta V||^2 + \alpha^2||\mathbf{R}(\sigma_0 - \sigma_r)||^2\}, \tag{3.53}$$

where $\mathbf{R}$ is a regularisation matrix that controls the smoothness of the solution, $\lambda$ is a scalar hyper-parameter that controls the amount of regularisation, and the value $\sigma_r$ represents the initial reference conductivity, which is not necessarily the same as $\sigma_0$. The regularisation matrix is usually assumed to be equal to the identity matrix $\mathbf{I}$. This choice allows to prevent extreme value of conductivity by properly tuning the penalty term $\alpha^2||\mathbf{R}(\sigma_0 - \sigma_r)||^2$, but it does not ensure smoothness or impose any constraint to the solutions. In the EIT imaging problem, conductivity in each element of the FEM mesh

is commonly assumed constant and similar in value to nearby elements.  To ensure such property a different regularisation matrix should be used. Possible solutions are the followings:

- *Gaussian-type prior* [60, 61]: an approach that penalise components with high spatial frequency in the reconstructed image by assuming higher correlation between neighbouring elements and a gradually diminishing correlation with increased distance.

- *Laplacian-type prior* [62]: this approach uses a discrete approximation of the Laplacian filter, which is a second-order filter that models the correlation between elements, smooth the solution, and penalise high spacial frequencies.

- *Newton's one-step error reconstructor* (NOSER) *prior* [63]: an algorithm that is based on the the first step of the Newton-Raphson method, and with the assumption that the conductivity is homogeneous.  The combination with the Tikhonov regularisation produces smoother results since the regularisation matrix is scaled according to the sensitivity of each element.

Despite the choice of the regularisation matrix, the formal equation of the problem (3.53) can be written as [28]:

$$\Delta\sigma = (\mathbf{J}^T\mathbf{J} + \alpha^2\mathbf{Q})^{-1}(\mathbf{J}^T\Delta\mathbf{V} + \alpha^2\mathbf{Q}(\sigma_r - \sigma_0)), \qquad (3.54)$$

where $\mathbf{Q} = \mathbf{R}^T R$. An alternative solution incorporates a weighting matrix $\mathbf{W}$ to model the noise variance between the potential measurements and then overcome noise in the potential measurements produced by faulty electrodes.  The full solution takes the form [53, 60, 61]

$$\Delta\sigma = (\mathbf{J}^T\mathbf{W}\mathbf{J} + \alpha^2\mathbf{Q})^{-1}(\mathbf{W}\mathbf{J}^T\Delta\mathbf{V} + \alpha^2\mathbf{Q}(\sigma_r - \sigma_0)) \qquad (3.55)$$

In the work presented here, it will be assumed that full data sets are available and all measurements have equal noise variance. The generalised Tikhonov regularisation (3.54) will therefore be used. In addition, since only the changes in conductivity will be measured, it can also be assumed that $\sigma_r = \sigma_0$. Then, for a fixed initial conductivity $\sigma_0$, the Jacobian $\mathbf{J}$ and $(\mathbf{J}^T\mathbf{J} + \alpha^2\mathbf{Q})\mathbf{J}^T$ can be precomputed off-line, improving the speed in the inverse resolution.

# Chapter 4

# System Overview

## 4.1 Introduction

In this chapter the mathematical description presented in earlier will be converted in guidelines and requirements for the development of the experimental hardware and software used in this work. For each developed component both the descriptive requirements that it has to satisfy, and the implementation will be presented.

Since the beginning of the work, it has been chosen to develop all the required components in-house. This was due not because of a luck of off the shelves technologies, but to have the full control o the single phase of the data acquisition and image processing. In addition, this allowed us to develop a more compact system than the one currently available on the marker that can be used in different situations.

In addition to the developed EIT hardware, in this chapter will be also introduced the conductive domain used in the experiments. This consists in two different structure: an artificial skin that has been used to test the feasibility and capability of the system under different scenarios; and a conductive silicon-based material that can be used in the developing of a soft deformable robot having embedded the sensing capability. By exploiting the idea of having a soft conductive robot over which it is possible to apply EIT as sensing technique, it is possible to overcome the current limitations related to the embedment of sensor within the soft device and thus obtain a shape-independent sensorised structure.

## 4.2 Hardware requirements

In the following section, the main requirements for the development of the developed portable EIT system will be provided. These can be organised into two main groups: one related to the requirements for the current source, and the second that summarise the requirements for the current injection and potential measurements system. Most of the decision made during the development were done in order to simplify the hardware design, and thus reduce its space in order to

develop a prototype that can be compatible in size and weight with a soft robot.

### 4.2.1 Current Sources

Most of the current sources used in EIT systems are more appropriately called voltage-to-current converters, since they produce an output current that is proportional to an input voltage. Ideally, Ideally, a current source should have an infinite output shunt impedance resulting in the current delivered to the load being independent of the load voltage. However, real sources have a finite impedance that is effected by the presence of the load. For this reason, the current source in an EIT system must be able to deliver current with a desired precision over a specified frequency range to load impedances within an expected range of values. While a higher level of precision is generally desired, current accuracy is also important. Higher accuracy can be obtained through current source calibration, where the current source is calibrated to deliver an accurate current to a test load having an impedance that is within the range of expected load impedances.

### 4.2.2 Current Injection and Potential Measurement

The hardware implemented to manage the driving patterns has to satisfy, the requirements defined as follows

- Bipolar current patterns are preferred over optimal patterns to simplify hardware implementation and to reduce cost and power consumption. A single current source multiplexed over multiple channels can be used with bipolar patterns.

- Non bi-directional DC current sources will be adopted; in order to ensure correctness in the measured data, potential measurements will be acquired after electromagnetic conditions have been stabilised.

- For bipolar patterns, potential measurements will be taken at all electrodes. However, potential measurements from the driving electrode–current source and sink–are not acquired in order to achieve a constant dynamic range in the data.

- Although in all the experiments it will be used the *adjacent* pattern, the ability to change between different bipolar patterns is desirable to give flexibility within the experimental EIT system.

## 4.3 Hardware for a Portable EIT System

Starting from this requirements, in this work we designed and developed a simplified version of a commercial EIT system to be used
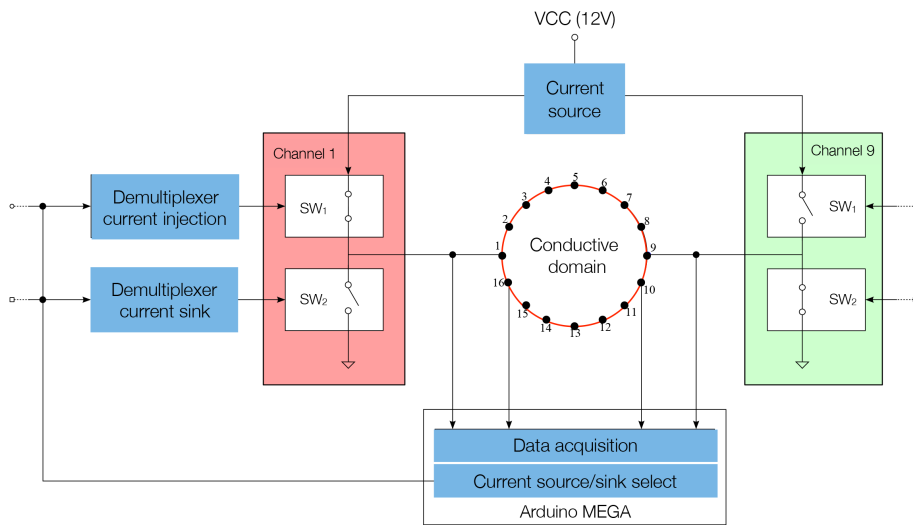
FIGURE 4.1: Schematic representation the EIT system.

as the main component of our sensing system. The main focus was places in developing a low-cost, adaptable system that is able to perform measurements by applying different patterns, and powered by a DC current source. The use of DC current simplifies the hardware requirements, and allow the use of the developed hardware even in battery-driven applications. The electronic system is composed by two main components printed on two separate printable circuit board (PCB): a voltage to current generator, and a driving/read-out circuit. Figure 4.1 shows a schematic representation of the developed EIT system.

The current generator, is implemented by a voltage regulator (Texas Instruments LM317) set up as precision current-limiter circuit. The output current value is controlled by a variable resistor, and it can be adjusted linearly by changing the resistor value. In order to provide a constant current supply on varying load, a voltage source of 12 V is used as input to the voltage regulator. The electrical current is then multiplexed across the different channels by the driving/read-out electronics. Each channel in the driving/read-out electronics is designed to operate at three independent stages. To provide such capability we implemented it as a half H-bridge where a n-MOSFET (International Rectifier IRLML6344TR) and a p-MOSFET (International Rectifier IRLML9301TR) are act as two independent switches connected to the same path. In such configuration, the p-MOSFET is connected to the positive source, while the n-MOSFET to the ground. By opportunely turning on and off the single switch, it is possible to set each channel to act as current source, current sink, or setting it to its high-impedance state in which the channel can be used to measure the voltage. As initial choice, the control of the driving/read-out electronics was performed directly by the microcontroller. In
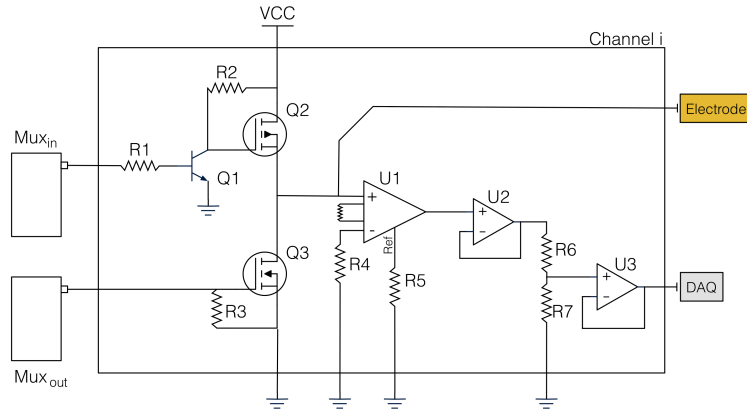
FIGURE 4.2: Schematic overview of the driving and readout electronics. The image depicts the configuration for a generic channel and its components. By using this configuration, a single channel can be set as: i) current source, ii) current sink (ground electrode), iii) or used to measure the voltage potentials respect an external, common ground. The process is controlled by the two independent de-multiplexer connected at each channel.

order to reduce the number of cables, and add modularity to the system, we moved to an integrated solution that use two independent de-multiplexer (Texas Instruments CD74HC237M). To capture the smaller voltage variation, we added to each channel an amplification stage. It consists in a low power, general-purpose instrumentation amplifier (Texas Instruments INA118) with variable gain. The output of this initial stage is referred to the ground. The signal then passes trough two subsequent op-amp (respectively Texas Instruments OPA827, and TLV2371) both configured in a non-inverting gain configuration. Figure 4.2 shows the structure of a single channel.

The driving/read-out electronics used in this paper has 8 independent channels. Although, the system has been designed to be modular to easily adapt its use to different requirements. Each channel is connected to the object under study by a single-ended cable that has at its extreme an alligator clip. The acquired signal is routed toward an analogue pin of the micro-controller (Atmel ATmega2560). Since each channel is measured independently, it is possible to perform any possible pattern combinations either at run-time or in post-processing. It is worth to mention that in the current version of the acquisition system no further processing of the signal, e.g noise filtering, or signal conditioning, has been performed. Figure 4.3 shows an overview of the developed electronics as an Arduino Mega2560.

A full set of potential measurements as obtained using bipolar
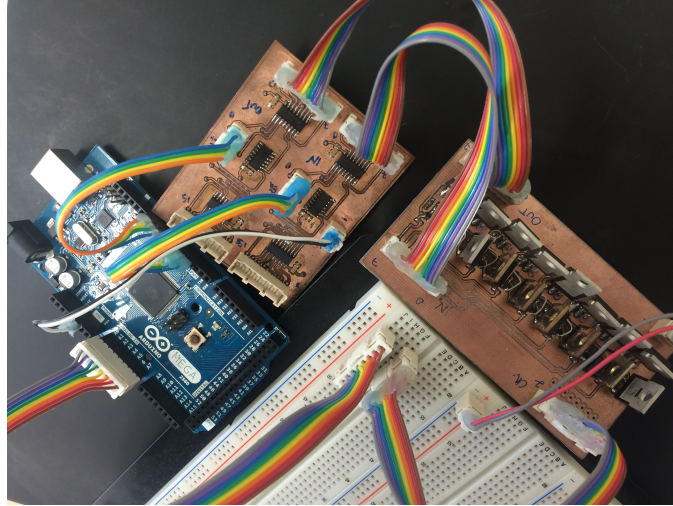
FIGURE 4.3: Developed EIT driving/read-out elec-
tronics connected to the micro-controller board.

drive patterns. In this technique electrodes placed at the bound-
ary are selected to inject the current, while potentials measurements
are acquired from the remaining electrodes. The electrode pair used
to inject the current is then sequentially changed with the next pair
and the process potential measurement is then repeated until all the
possible combinations have been applied. The frequency of data ac-
quisition was configured through the ATmega2560 micro-controller
around 10kHz. To guarantee static electromagnetic conditions, a
suitable experimental determinate short delay ($\tau \approx 2$ms.) was incor-
porated after each current injection step. To improve signal-to-noise-
ration, an oversampling technique was implemented by acquiring
multiple potential measurements from all boundary electrodes and
averaging before switching to a new pair of current-injection elec-
trodes.

## 4.4 Reconstruction Software

A user interface for experimental control and for the real-time in-
verse solution and image reconstruction were written in Matlab®.
Although Electrical Impedance Tomography and Diffuse Optical To-
mography Reconstruction Software (EIDORS) [62] was used for ini-
tial testing, most of the experimental software was designed and im-
plemented by the author. This provided better control of the software
and all desire changes that were required for this robotic application.

Figure 4.4 shows a flow chart of the software implemented. From
that, it is possible to notice that the user interface is used to configure
all parameters and control of data acquisition and real-time visuali-
sation. Some of the main properties are the following:

- The *geometry* of the domain can be selected among a predefined set of shapes.

- *Electrodes* can be set up to sixteen in accordance with the hardware design.

- *Mesh size* used in the solving the inverse problem can changed in order to control the number of elements of the FEM and thus adjust its resolution.

- The initial homogeneous *resistivity* of the domain required for modelling and solving the forward problem.

- The contact *impedance* can be set to improve the accuracy of the model. However, since difference imaging is used, only an approximated value is required. In fact, any error in the inverse solution are cancelled out.

- *Injection*, and *measurement* patterns can be chosen, and can be further added by the user. Additionally, the *algorithm* for the inverse solution, and the regularisation prior can be selected accordingly a predefined set.

- The value *alpha* of the hyperparameter that control the smoothness of the regularisation.

Once the parameter are set, the algorithm proceed in creating the forward model. Once the model is set, the Jacobian $\mathbf{J}$ and $(\mathbf{J}^T\mathbf{J} + \alpha^2\mathbf{Q})^{-1}\mathbf{J}^T$ in Equation 3.54 can be computed from the assumed homogeneous conductivity distribution. All quantities, at this point, can be calculated off-line increasing the speed in the inverse resolution.

In this work, difference imaging has been used. This technique requires the acquisition of two sets of potentials, $\mathbf{V}_1$ and $\mathbf{V}_2$, taken at two distinct time steps. The change in the potentials, $\Delta\mathbf{V}$, is then used to determine the variation in conductivity, $\Delta\sigma$, of the domain. A first set of potential $\mathbf{V}_1$ is acquired and stored as an initial reference. The inverse problem is then solved inside a infinite loop in which $\mathbf{V}_2$ is constantly updated with the acquired measurements. Within the same loop it is possible to display the reconstructed conductivity, and to store the acquired data for later off-line processing. For display purpose only, a two-dimensional circular averaging filter was used after image reconstruction to reduce the stepwise changes caused by the FEM approximation.

The rate of the image reconstruction depends on the complexity of the problem, which is linearly dependent on the elements in the Jacobian matrix $\mathbf{J}$. As stated in the Nyquist sampling theorem, any dynamic contact that contain frequency components exceeding one half of the reconstruction frequency rate, can not be accurately determinate.
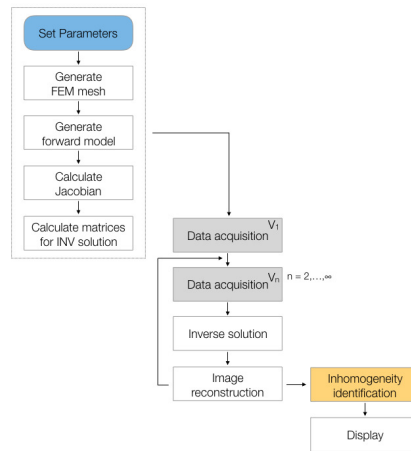
FIGURE 4.4: Flow chart of the experimental EIT software. Data acquisition stage (grey boxes) is described in detail in Figure 4.5
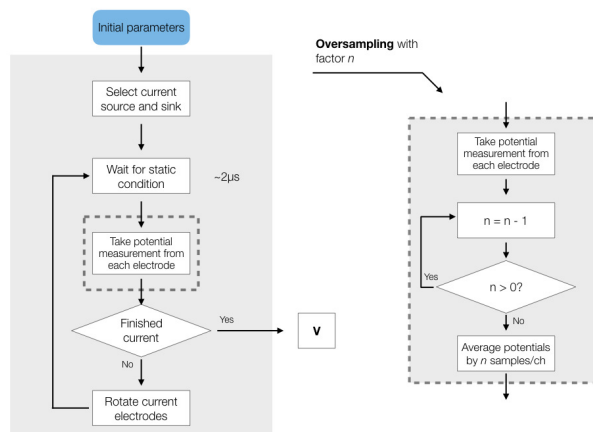


FIGURE 4.5: Flow chart of the EIT data acquisition stage for a full set of potential measurements both with, and without, the over-sampling stage.

## 4.4.1 Metrics for Reconstruction Evaluation

It is not trivial to assess the quality of the EIT reconstructed image. In fact, EIT imaging performance depends strongly on the reconstruction algorithm and its parameters. To minimise bias when investigating driving patterns and verify that that improvements to the EIT reconstruction are available, several commonly used regularisation methods and hyperparameter values were compared. Several metrics [51] [64] [65] have been used in order to measure qualitative measure the reconstructed image. In this work three metrics—in addition to the *maximum intensity value*—previously used un medical imaging have been used.

### Maximum Intensity

This metric is calculated as the value of maximum intensity of conductivity change in the reconstructed image. A desired behaviour to achieve is a constant intensity change, due to the same stimulus at any position across the conductive domain.

### Spatial Resolution at 50% of Image Amplitude

This value ($RES_{50}$) is calculated by evaluating the ratio between the number of elements in the reconstructed image having value at least 50% of the maximum amplitude, and the total number of elements in the mesh.

$$RES_{50} = \left( 1 - \sqrt{\frac{\text{Elements over } 50\% - 1}{\text{Total Elements}}} \right) \tag{4.1}$$

The metric is similar to the ones proposed in Adler and Guardo [51] and Wheeler et al. [65]. With the increase of the spatial resolution, the system is able to discriminate between different stimuli rather than to identify them as a single one. EIT has a low spatial resolution, when compared to other imaging techniques, that affects its ability to correctly discriminate between stimuli. For this reason, the technique is not suitable for applications where high spatial resolution is required. In a soft robot, stronger pressures mask weaker ones, and as a consequence it is non trivial to discriminate when two distinct events occur at the same time.

### Shape Deformation Angle

By properly comparing the difference between its $RES_{75}$ and its $RES_{50}$ spatial resolution—where $RES_{75}$ is similar to the measure just introduced with the main difference in the threshold used—it is possible

to derive a measurements that evaluate the sharpness of the reconstructed image. The angle $\beta$ can be obtained as follows:

$$\beta = \tan^{-1}\left(\frac{25\% \text{ of max amplitude}}{(RES_{75} - RES_{50})/2}\right) \qquad (4.2)$$

In a discontinuous reconstruction, $RES_{75}$ is expected to be equal to $RES_{50}$, hence $\beta = 90 \deg$. The metric is based on the shape deformation metric based on the difference between two assumed circular areas presented in [64]. Here the assumption of circular reconstructions is removed and only the absolute differences are computed. The metric is calculated as an angle since this provides additional information about the overall shape.

**Distance Error at 75% of Maximum Image Amplitude**

The distance error ($ERR_{75}$) was evaluated by computing the Euclidean distance between the centroid of the stimulus $(x_1, y_1)$ and the centroid of the reconstructed image $(x_2, y_2)$. Only those elements in the reconstructed image containing at least 75% of the maximum amplitude were considered

$$ERR_{75} = \sqrt{(x_1 - x_2)^2 + (y_1 - y_2)^2}. \qquad (4.3)$$

A distance error value of zero ($ERR_{75} = 0$) would represent a perfect performance of the inverse solver. Similarly to the metric that measure the spatial resolution, the accuracy of this distance error varies with a series of parameter such as the patter used to inject the current and to measure the potentials, and the number and location of the electrodes used.

## 4.4.2 Image Processing and Data Analysis

The just mentioned metrics can be used to extract the position and peculiar information of a single inhomogeneity that has been detected in the reconstructed image. In case more than one event occur over the sensitive surface, additional processing is needed in order to identify each of those and the retrieve information from them. This processing does not affect the reconstructed image, it has only be used to identify the position and area of the detected inhomogeneities.

Each of these can be describes as a point spread function (PSF), such as the response of an imaging system to a point source or point object. In this context, due to the low resolution of the imaging technique, the PSF can be seen as the extended blob in an image that represents an unresolved object. As in the typical application, the degree of spreading (blurring) of the point object is a measure for

the quality of an imaging system. These considerations allow to apply common technique used in these situation. Figure 4.6 gives an overview of the method applied to achieve this task.

The starting point if the reconstructed image, and the process of detecting the peak of the single inhomogeneities. In order to proceed in the identification, an initial thresholding with respect to the maximum amplitude is performed. The value of the threshold $\Gamma_1$ is set accordingly to the case, but experimentally values ranging between 60% and 70% of the maximum pixel intensity have be proven to be a good choice. In order to reduce the steepness of the FEM discrete approximation, a gaussian filter is applied on the thresholded image followed by a second thresholding $\Gamma_2$ in which only the pixel having more than 90% of $\Gamma_1$ are selected. Simple thresholding process, as the one described so far, are not enough to clearly distinguish between inhomogeneities that are relatively close each other. To better identify these an additional step is needed.

Once the thresholded image is returned, the peak of each detected region are identified. Two are the possible approaches to perform this task. The first consists in scanning all the detected pixels and select only the ones that have value greater that the ones of the neighbouring pixels. The process is robust, fast—linear with the number of detected elements—and has the advantage of identifying with high probability the "true" PSF local maximum. The second approach is based on the use of weighted centroid. This approach uses the same image processing, with the difference that it just calculated the weighted centroid of each connected object that was obtained following the image processing. While this gives sub-pixel resolution, it can miss peaks that are very close to each other, and runs slightly slower.

## 4.5   Development of the Conductive Layer

In this section the development of the conductive substrate used in the experiments performed in this work. In order to allow full adaptability of the system we decided to develop a conductive domain. The main prototype has been developed by layering a conductive textile over a thin foam substrate was used to evaluate the performance of the system in different scenarios. Details about the development and the properties of the material used will be discussed in the following section.

### 4.5.1   Skin Fabrication

The properties of the material that is used to form the EIT-based skin are crucial to its performance. An ideal material would have continuous and homogeneous conductivity, give large, linear and local
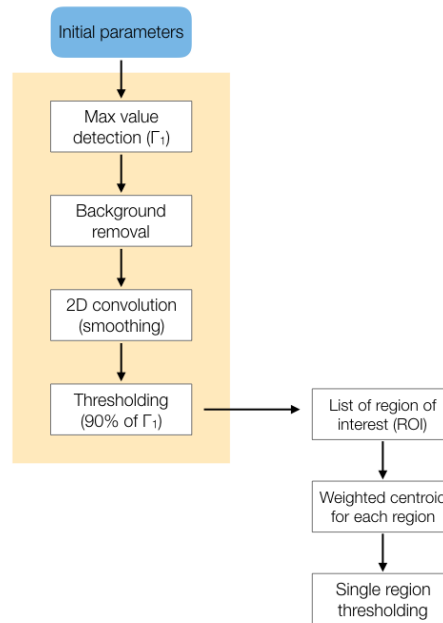
FIGURE 4.6: Schematic overview of the process used to identify single inhomogeneities detected over the reconstructed image.

changes in conductivity in response to forces applied normal to the surface, and have no conductivity change as a result of stretch. Cost should be low. A number of materials were investigated with the aim of finding one with the better properties. To the writer's knowledge there are no suitable materials that are commercially available, so a custom-made material was necessary.

Initial experiments were performed with an inexpensive four-way knitted conductive fabric manufactured by Statex (Figure 4.7). This material is a highly conductive (surface resistivity $\Omega < 1$ ohm/sq), medical grade silver plated 78% Nylon 22% elastomer fabric with the ability to stretch in both direction (maximum stretch $\approx 100\%$ in length and $\approx 65\%$ in width). The conductivity of the material chances when it is stretched in-plane, or when a normal force is applied over the textile surface. The phenomena is due changes in the contact area between the sings that compose the structure of the fabric. In fact, when the fabric is stretched, the increased separation between conductive strings causes a non-linear reduction in contact area and—as a result—a non-linear decrease in conductivity. Compression of the fabric has the opposite effect, although greater conductivity changes were observed due to stretch.

Sheet resistance is used when measuring the resistance of thin films of conductive materials that are nominally uniform in thickness. Values are typically expressed as "Ohms per square" (Ohm/sq) to emphasise that the resistance is independent of the size of the sample. The term conductivity, as opposed to resistivity, will be used

FIGURE 4.7: Conductive stretch fabric from Statex.
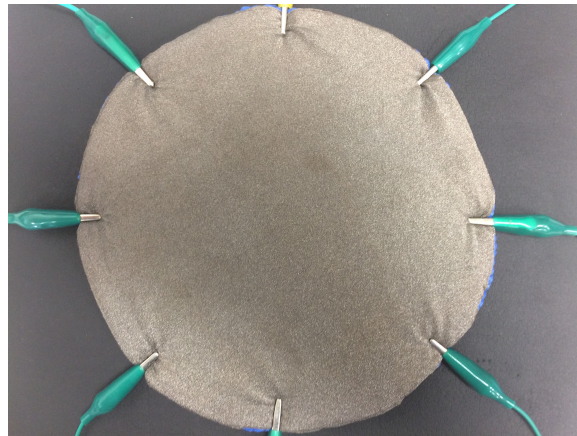


FIGURE 4.8: Experimental conductive substrate (grey textile) made by layering a conductive textile over a thin foam material (blue material). The structure has been then attached to eight stainless alligator clip used as electrodes.

here for consistency with the EIT mathematical model and the literature. The terms conductivity and surface conductivity—in Siemens per square (S/sq)—will be used interchangeably when referring to thin conductive fabrics.

A prototype circular sensitive skin was made by positioning eight stainless steel bolts used as electrodes around a circular piece of the conductive textile of 200 mm diameter, as can be seen in Figure 4.8. As electrodes, eight stainless steel bolts were used and fixed near the edge of this layer. A constant DC current was injected across adjacent pairs of electrodes and potential were taken at all the electrodes using the same adjacent pattern. Due to the high conductivity of the cloth, 100 mA of current was required to achieve acceptable potential levels at the boundary. Since greater changes were observed due to stretch in comparison to pressure, a non-conductive foam was used under the fabric to increase fabric stretch as a result of pressure. The complete electrode model and a Gaussian-type regularisation prior were used for inverse solution.

# Chapter 5

# Performance Evaluation

## 5.1 Introduction

In this chapter the initial system performance evaluation will be presented. Initial experiments were carried out with the hardware described in previous chapter, and by using the textile-based conductive domain. The system has been tested under different configurations spanning from data acquisition to test the basic measurements protocols, to the application of the sensor around curved surfaces to prove the adaptability of the method. In the following sections, for each tested scenario will be presented both the experimental setup, and the related experimental protocol used to perform the test.

## 5.2 Experimental Evaluation

In this section, we are going to present the experimental setup used to characterise the behaviour of the sensor under different scenarios. In a first phase, electric potentials are acquired both in absence and in presence of different loads applied over the artificial skin. These initial measurements are fundamental to create a series of reference values for the conductivity reconstruction. In a second phase, we applied the reconstruction algorithm to prove the capability of the system to correctly identify the presence of the probe and its position. In the last phase, more complex interactions – as multi-touch identification, and application over curved surfaces – were addressed to prove the artificial skin capabilities.

### 5.2.1 Experimental Setup

The experimental setup employed for the characterisation of the smart skin system consists of the components schematically illustrated in Figure 5.1. The artificial skin is connected to the driving/readout electronic previously described. This is controlled by an external ATmega2560 powered micro-controller that is used to both switch the status of the different channels, and as data acquisition board (DAQ). A laptop with Matlab installed is connected to the micro-controller
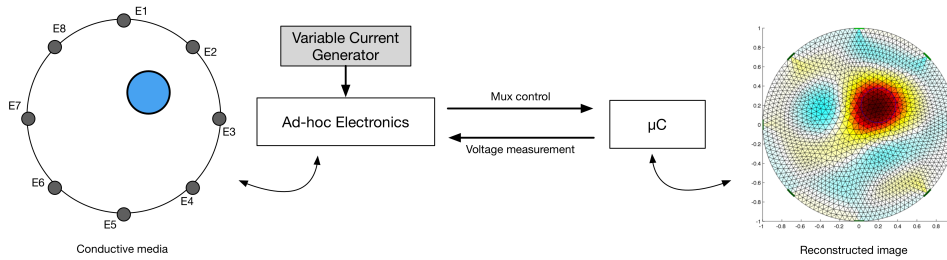
FIGURE 5.1:  Schematic view of the experimental
setup. The artificial skin is connected by wire to the ad-
hoc developed driving/read-out circuit.  This is con-
nected to a microcontroller that sets the status of the
different channel, and functions as a digital acquisition
board. The whole system is then connected to a laptop
on which the main program and the inverse solver are
running.

and used to control the whole system, and to perform the inverse
problem solving.

To prove the adaptability of the system to react and detect var-
ious stimuli, we used different probes that vary in size and shape.
For instance, we used 3 different circular probes with radius ranging
from 15mm to 25mm, and a square head probe with a side of 15mm.
In all the experiments, in order to cope possible fluctuations of the
acquired value, a series of 10 measurements have been acquired and
then the mean value is used. In all the experiments, unless differently
stated, the artificial skin was placed on a flat surface.

For the reconstruction process, we used a dynamic imaging ap-
proach.  A reference measurement was acquired and stored to be
compared with later ones. Although the EIT community is moving
toward a unified approach to reconstruct 2D medical images [64],
as inverse solving algorithm we used the Gauss-Newton EIT recon-
struction approaches, which have been widely used in EIT since the
late 1980s [66].  The approach allows to represent the solution as a
linear reconstruction matrix, which can be pre-computed and thus
allows rapid, real-time imaging. The parameter used for the inverse
solver were derived empirically by measuring the error of the recon-
struction using different probes and then by selecting the best solu-
tion.  In order to provide consistency in the reconstruction, the pa-
rameter values remain the same during all the experiments, unless
otherwise stated.

## 5.2.2   Experimental Protocol

Different tests were performed to assess the overall performance of
the sensors, according to the following protocols.

**Preliminary Analysis on the Sensor Working Principle**

A first series of experiments has been performed in order to capture the output value of each electrode in absence of any force applied over the sensing area. At first, the output of an arbitrary chosen electrode was directly monitored and acquired with Matlab during a full driving cycle. In order to obtain valid measurements, we waited a fixed amount of time of $2\mu s$ (empirically found) to ensure electromagnetic stability before acquiring the data. The obtained value can be considered as the offset for the voltage potential measurements to be used in later phases where differences in the measured data correspond in presence of inhomogeneity within the sensing layer due to external stimuli (i.e. touch or stretch).

**Indentation Tests and Electrode Sensibility**

Following the results obtained in the first series of experiments, we continue by evaluating the changes in conductivity as a function of size and position of different loads applied over the sensing area. In order to better understand this phenomena, we applied the probe in the region directly facing each electrode. The test were performed using different probes with different sizes, and shapes while maintaining constant the applied force. For each configuration, we acquire the data 10 times and then averaged them to obtain a more stable waveform. Two of the results are shown respectively in Figure 5.5 and 5.6.

**Pressure Map Reconstruction**

The artificial skin functionality was validated by means of indentation tests with the different probes as indenter. The measures obtained in the previous experiments were then used to tune the inverse problem solver and then reconstruct the conductivity map associated with the artificial skin. The series of experiments were aimed to prove the capabilities of the inverse solver in detecting the position and size of the different probes used in the tests. Once the reconstruction has been performed, to identify the position and the area associated to the inhomogeneity we perform first a peak detection to identify the point with maximum intensity, and then a thresholding according to the peak value. In this phase we only consider single events that occur over the surface.

**Multi-Pressure Test**

To prove the capability of the artificial skin in detecting multiple contacts at the same time, the system was placed on a flat surface, and different contacts were achieved on its sensing area by means of hand-held probes with a circular section. Each loads was added

sequentially, and then removed in the same order. During the experiment we did not consider the nominal force applied on each probe. Additional test to improve object discrimination capabilities and pressure measurements will be left as future work.

**Application over Curved and Deformable Surface**

With a last series of experiments we wanted to prove the adaptability of the artificial skin to different substrate, in particular to curved and deformable ones. In order to proceed in this direction, we first placed the artificial skin over different cylindrical surfaces with different radius. Afterwards, we placed the sensor over other objects such as a bendable mannequin arm, the back of a chair, and around a deformable foam-made cylinder. Where the underlying object did not provide sufficient support for the artificial skin, we placed the object over a table. Once the artificial skin was applied over these geometries, we performed similar experiments as in the case of the flat surface ones. During these test, we focused or attention on: i) the capability of the system in detecting a change of shape, ii) and the robustness of the sensing technique even under large deformations. In the first case, we used as reference voltage the ones taken on a flat surface and we compared those with the one taken when the sensor was wrapped around the curved surface. In the second case, instead, both the reference and later measurements were taken directly when the artificial skin was placed over the curved surface.

## 5.3   Results

The results of each single experiments are reported in the following sections subdivided by their respective categories.

### 5.3.1   Working Principle and Material Characterisation

Initial tests have been performed to understand the behaviour of the conductive material – used as sensing layer – when an electrical current flows through it. Due to the high conductivity of the material ($< 1\Omega/$sq.), 100 mA of current was required in order to achieve an acceptable voltage potential levels at the boundary. In the future version of the sensor we are planning to move to a more resistive material in order to reduce the electrical current required for the system. During the characterisation process, no physical contact or force was applied over the sensing area of the smart artificial skin. Figures 5.2 and 5.3 show the voltage potential measurements, respectively at electrode 3 and 6 during a full cycle of excitations. The values were acquired using adjacent patter, thus each value in the graph represents the potential calculated between two adjoining electrodes. As the measurements suggest, the maximum and minimum variations
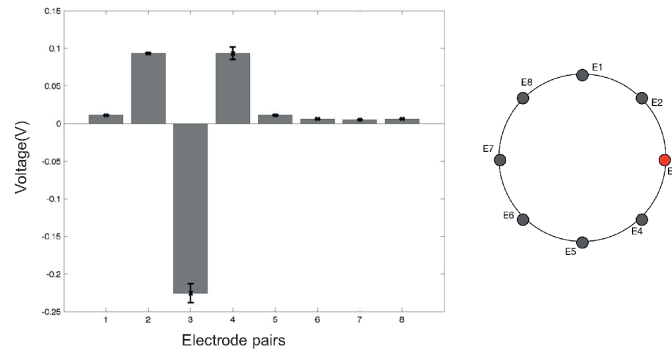
FIGURE 5.2: Electric potentials measured at electrode 3 (E3) in an 8-channel configuration. Measurements are taken using an *adjacent pattern* both in excitation and acquisition phase. The positive peaks corresponds when the electrode is "close" to ground nodes. On the contrary, the negative peak occurs when E3 is used as current sink. Error bars show the variability of measurements calculated over 10 samples.

can be found when the driving electrodes are close to the one where the measurements were taken. The assemble of all the measurements acquired from all the electrodes represents a reference voltage, $V_0$, used to calculate differences in the electric potentials when an event occurs over the sensor surface. Figure 5.4 shows an example of the reference measures.

## 5.3.2 Single Point Contact - Signal Indentation

Using the same electrode configuration as in the previous experiments, we evaluated the changes in the acquired electric potentials as a consequence of an applied load over the sensing area. To better notice the phenomena, we chose the position of the probe 5-10mm apart from to the electrode under test. For this specific test we used only one probe with circular section (15mm radius) over which we applied a constant force of 3N. By simply comparing the measurements in presence and in absence of the applied load is not possible to clearly appreciate the difference between them. A more clear understanding is noticeable by considering the absolute variation $(V_{meas} - V_0)$ between the two measurements. Figure 5.5 shows the absolute difference using the value acquired by electrode 2 (E2) when the probe was paced in the region facing the electrode. In the figure, the different measurements are grouped according to the electrode acting as ground. Each bar represents a voltage difference computed over adjacent electrode – e.g. the first bar refers to electrodes E1-E2, the second to E2-E3, and so on until all the electrode pairs are considered. Shaded regions are not to be considered since the electrode under consideration was acting as current source or connected to
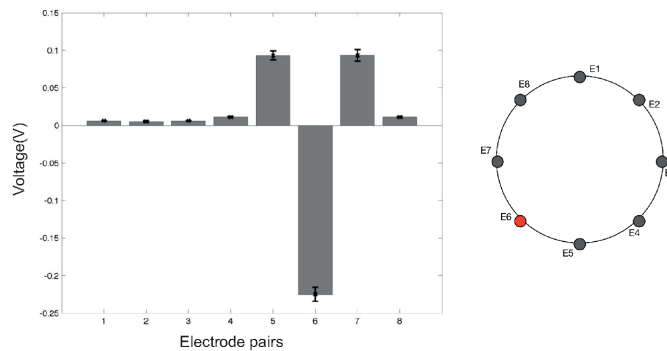
FIGURE 5.3: Electric potentials measured at electrode 6 (E6) in an 8-channel configuration. Measurements are taken using an *adjacent pattern* both in excitation and acquisition phase. The positive peaks corresponds when the electrode is "close" to ground nodes. On the contrary, the negative peak occurs when E6 is used as current sink. Error bars show the variability of measurements calculated over 10 samples.
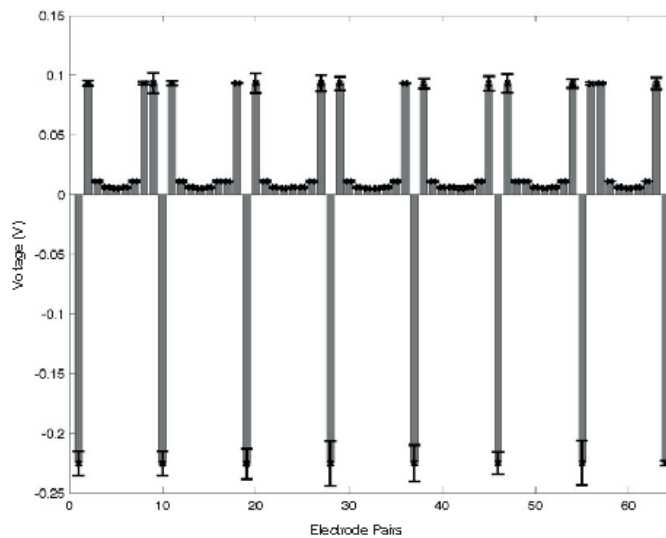


FIGURE 5.4: Electric potentials measured at each electrodes pair by using an adjacent pattern both in excitation and acquisition phase. The measurements were taken when no load was applied over the artificial skin.
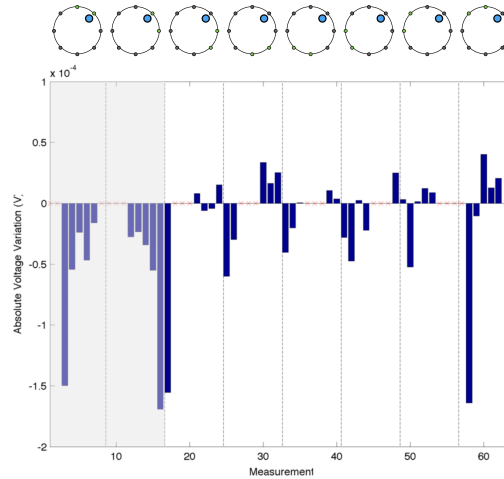
FIGURE 5.5: Electric potentials measurements acquired when a probe is acting in the region facing the electrode 2 (E2). The values are grouped by which electrode is used as ground following an adjacent pattern (highlighted in the top part of the figure). The shaded portion of the graph corresponds to the configuration when E2 is one of the driving electrodes. The major noticeable differences are the ones when E2 is involved in the measurements.

ground. In the figure, major negative changes occur in the electrode pairs that involve E2 (i.e. first 3 bars in each group). The changes are a consequence of the presence of the probe that, acting on the conductive surface, changes the local conductivity of the layer. Is possible to notice a similar patter when any of the other electrodes are considered. As reference, Figure 5.6 shows the absolute voltage potential when a load was acting in the region facing the electrode 7 (E7).

Considering the same electrode configuration, we evaluate the changes in the absolute voltage variation as a function of the probe size while applying a constant force (5 N) over them. Three different circular probes with radius of 15mm, 18mm, and 25mm were placed independently in front of the region facing electrode 4 (E4). Figure 5.7 shows the results of the experiments. As the graph suggests, with the increase of the probe size, the variations of the voltage potential increase. The phenomena was expected since a larger probe generates a wider inhomogeneity area that is the cause a consequent voltage drop. Even if the probe size is changed, it is still possible to notice a large negative change in the electric potentials when E4 is considered in the measure. Similar effects are expected in the case where the probe area remain constant and the applied force is increased. This consideration requires additional verification that is left as future work.
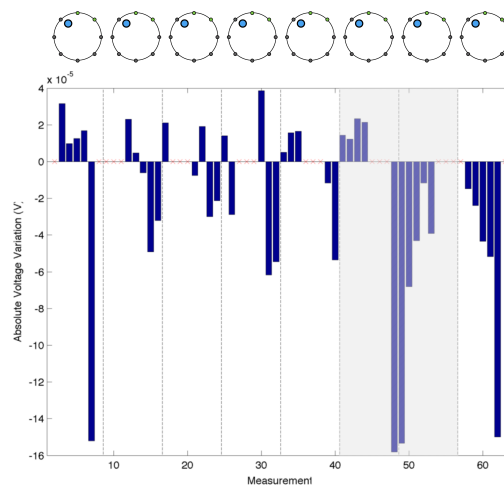
FIGURE 5.6:   Electric potentials measurements acquired when a probe is acting in the region facing the electrode 7 (E7).  The values are grouped by which electrode is used as ground following an adjacent pattern (highlighted in the top part of the figure).  Not considering the region where E7 is acting as driving electrode (shaded area), the major noticeable differences are the ones when E7 is involved in the measurements (i.e. last two bar in each group).
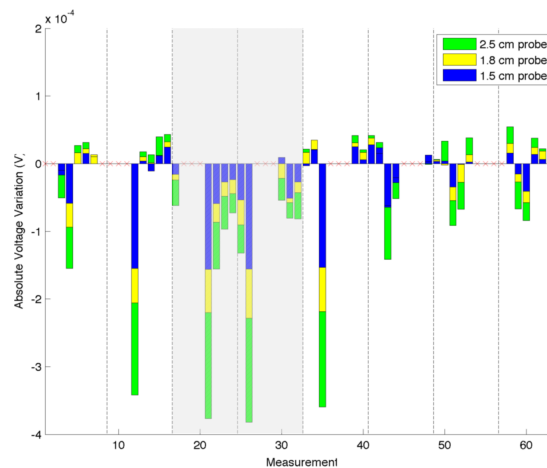


FIGURE 5.7: Difference in electric potentials measured when different probes are placed in the region facing electrode 4 (E4). The probes have different size, while the applied force is kept constant.  As in the previous image, the shaded regions correspond to E4 acting as driving electrode.

### 5.3.3 Conductivity Map Reconstruction

In this phase, we validate the capabilities of the inverse solver to reconstruct the pressure map of forces acting over the sensing area of the artificial skin. As previously introduced (Section 5.2), in order to guarantee the solvability of the inverse problem, we precondition the solution using NOSER (Newton's one-step error reconstructor) Gauss-Newton normalised difference inverse. For the initial test, we used a single circular probes with radius of 18mm, and applied it in different regions of the sensing area. Figures from 5.8a to 5.8c show the results obtained though the reconstruction algorithm. It is worth to say that no filtering of the data has been performed during any phase of the process. In the image, the inhomogeneity is clearly distinguishable from the background but its shape is not well defined. As the images suggest, the closer the object is placed toward the centre of the sensitive area, the interaction between the applied force and the constraint produced by the electrodes is reduced (Figure 5.8c). On the opposite, the more the probe is placed toward the boundaries, and thus closer to the electrodes, the reconstructed shape of the probe results to be less precise. This can be caused by the effect the pressure has over the applied point and the constraints due to the presence of the electrodes. To partially overcome this issue, we processed the reconstructed map by thresholding it and considering only the pixel having value up to $70\%$ of the detected maximum value. Figures from 5.8d to 5.8f show the reconstructed conductivity map with superimposed its centre.

We also tested the inverse solver capabilities to distinguish different probe shapes when applied, independently, over the same position. In order to have less interaction with the boundaries, that have proven to suffer from a highest distortion due to the interaction of the probe with the electrode, we decided to use the central region for the tests. Figure 5.9 shows the results of the reconstruction using the 3 circular probes, and a square one under the effect of a constant force of 3N. Due to the intrinsic low spatial resolution of the EIT method in this region it was not possible to clearly discriminate between the sharp-edged probe (Figure 5.9d) from the rounded-edged ones. Nevertheless the change in the probe size (Figures 5.9a-5.9c) can be clearly identified as the increase of the detected maximum value when a common colour scale is used.

### 5.3.4 Multi-Pressure Test

Following the experimental design described in the previous sections, we tested the capabilities of the artificial skin in the detection of multiple events that occur sequentially and simultaneously over the sensing area of the artificial skin. Three probes with the same size and shape (circular section with 15mm of radius) were manually placed and then removed sequentially over the sensitive surface

|        |        |        |
|:------:|:------:|:------:|
| (A)    | (B)    | (C)    |
| (D)    | (E)    | (F)    |
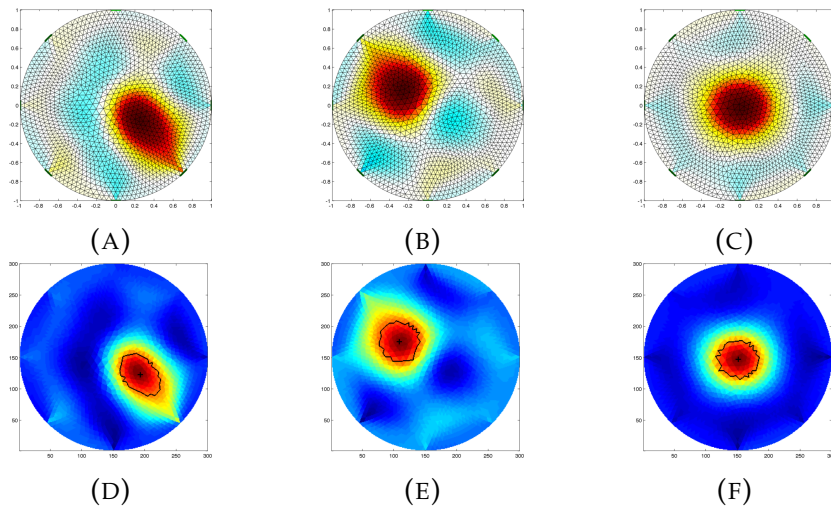
FIGURE 5.8: Reconstructed conductivity map of different stimuli applied over the artificial skin by a circular head probe of 18mm of radius. The probe was placed (a) between electrodes E3 and E4, (b) between electrodes E7 and E8, (c) in the centre of the sensing area. Figures (d), (e) and (f) show the processed data respectively of figures (a), (b), and (c). In each of the processed image, the centre and the computed boundary of the detected inhomogeneity and are shown.



|     |     |     |     |
|:---:|:---:|:---:|:---:|
| (A) | (B) | (C) | (D) |
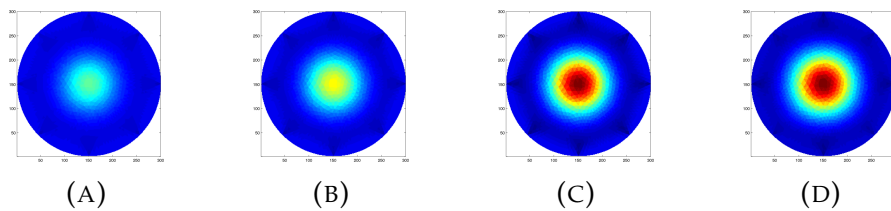
FIGURE 5.9: Reconstructed image as function of different probes applied at the centre of the artificial skin. The results provided are respectively for: (a) a circular probe with 15mm radius, (b) a circular probe with 18mm radius, (c) a circular probe with 25mm radius, and (d) a square probe with a side of 15mm. Due to the low resolution of the system, it is not possible to clearly discriminate between the different shapes. Nevertheless the change in the probe size can be easily identified.
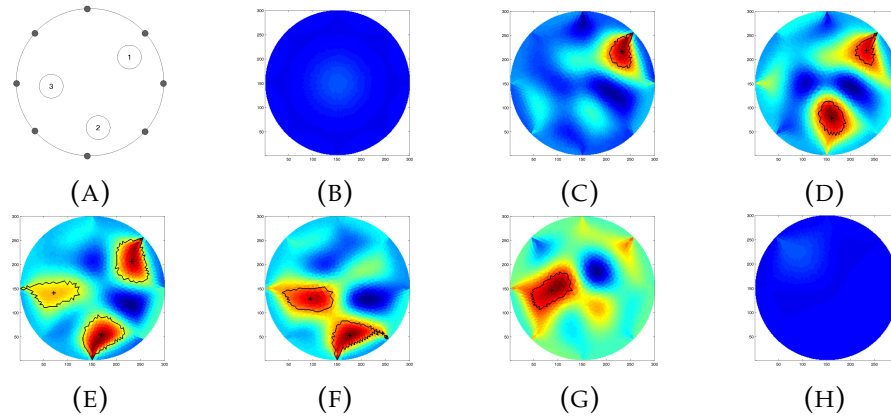
FIGURE 5.10: Selected frames in the multi-pressure experiment. (a) Probes positions, (b) reference voltage, (c)-(e) sequential load and (f)-(h) unload of the different probes. In each frame, for each probe, its centroid and the computed boundaries are shown.

of the artificial skin. In order to ensure the equal applied force, a mass of 400g was placed over each probe. As in the previous case, no signal processing has been performed prior or during the image reconstruction; the only operation that was performed was the pre-condition of the solver to ensure solvability. In Figure 5.10, selected frames obtained trough the reconstruction process are presented.

As in the previous cases, we processed the conductivity map to obtain the area where each probe was acting. We first applied the same methodology as in the precious cases, but we were unable to correctly identify the third probe when it was places over the sensing area together with the other two (Figure 5.10e). For this reason, we reduced the threshold value from $70\%$ of the maximum value to its $60\%$ value. As the images suggest, the shapes of the probes could not be correctly detect as a consequence of the position and the interaction of the electrodes. In addition, the artificial skin shows some hysteresis after the removal of all the probes. This can be caused by the partial detachment of the conductive textile from its substrate, and by the change of conductivity of the sensing layer as a consequence of the applied forces.

### 5.3.5 Application over Curved Surface

A last series of experiments was carried out to prove the adaptability of the artificial skin to conform to different geometries while maintaining its sensing property. Furthermore, is also possible to test the efficiency in determining changes in shape (e.g. bending) due to the application of the artificial skin over different geometries and comparing the acquired electric potentials with the ones acquired over

(A)  (B)
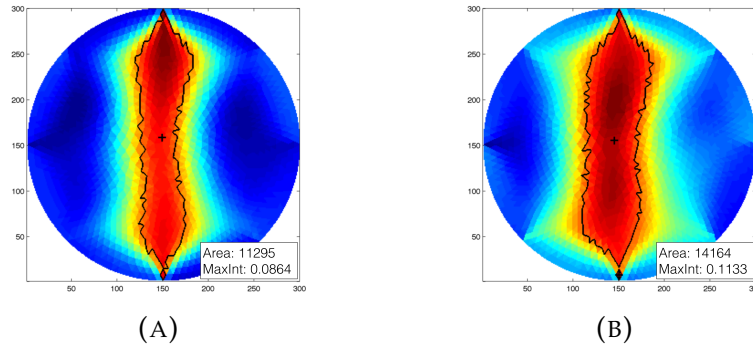
FIGURE 5.11: Results of the application of the artificial skin over a curved surface. The reconstructed conductivity map was generated by using as reference the measurements taken over a flat surface with no load acting over the artificial skin. In this experiment we used two polyethylene foam extruded cylinders with diameter of (a) 40mm, and (b) 70mm. As the results suggest, as the diameter of the underlying object increase, the maximum intensity and the area of the detected inhomogeneity increase.

a flat surface. In this section we are going to present the results obtained after the application of the artificial skin over different curved and deformable objects.

As initial test, we placed the artificial skin over a flat surface and then took a series of voltage potential measurements. With those value stored as reference, we placed the artificial skin over different cylindrical objects – two polyethylene foam extruded cylinders – with radius, respectively of 40mm and 70mm. The two cylinders were then placed over a flat surface in order to provide sufficient support, and avoid their bending. Due to the presence of the foam substrate, and the small size of the underlying object, the artificial skin could not conform perfectly to it. Thus, in order to fully cover the cylindrical object, we kept the two free side of the artificial skin together by means of plastic strip. In such configuration, we performed the electric potentials measurements. Figures 5.11a and 5.11b show, respectively, the results for the two different cylinders. The reconstructed conductivity maps presented in the two figures shows a different behaviour compared to the one saw in the previous experiments. In fact, instead of having a ellipsoidal region, this type of deformation produces a more elongated one. By comparing the images in Figure 5.11, it is possible to notice a slight change both in the maximum value detected, and in the computed deformation area – obtained as in the previous cases by thresholding the reconstructed map. These information can be used as clue to discriminate between different type of deformations applied to the artificial skin.

Following the results obtained in the first part of the trials, we further test the artificial skin capability to sense pressure when placed on curved geometries. We evaluate such property on the following objects: a 70mm radius cylinder (deformable), the back of a chair (soft substrate), and a mannequin arms with circumference of 30mm and a total length of 295mm. Before proceeding with the measurements, we firmly attached the artificial skin to the underlying object in order to limit the error in the reconstruction due to changes in the electrode positioning. Where the object was not able to support itself, i.e. in the polyethylene foam extruded cylinder case, we placed the object of a flat surface during the whole test. We limit the experiments to a single probe of circular section and 18mm radius. Differently from the precious case, reference measurements were taken after attaching the artificial skin on the curved surface. Results for each configuration are shown in Figure 5.12. As the images suggest, the artificial skin can provide similar results as the ones shown in previous cases even under large deformations.
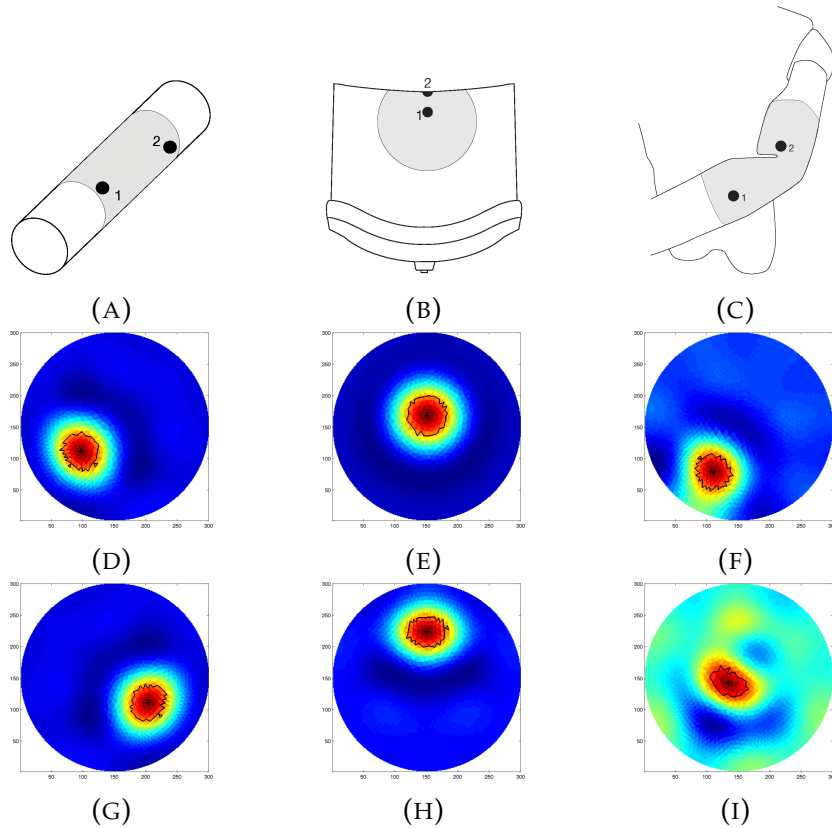
FIGURE 5.12: Example of conductivity map reconstruction over different geometries, results are grouped by column. First column (a, d, g) experimental setup and results when applied to a 70mm radius cylinder (deformable). Second column (b, e, h) experimental setup and results when applied to the back of a chair (soft substrate). Third column (c, e, i) experimental setup and results when applied to a mannequin arms with circumference of 30mm (bendable). Results are ordered according to the number shown in their relative experiment setup. Last row of the Figure shows measurements performed when the probe was applied over the most curved area (g, h), and when the joint angle of the mannequin arm was changes (i). For each case, the results are obtained by applying a circular shape probe with 18mm of radius.

# Chapter 6

# Applications

## 6.1 Introduction

In this section we are going to extend the results obtained in the previous series of experiments to possible applications for the developed technology. We tested the system in two possible scenarios, one related to sensing structural changes of the underlying structure, and the other related to a possible medical application. As in the previous cases, for each scenario will be presented the experimental setup and protocol, the aim of the experiment, and its results. Despite this, we believe that it is possible to use such technologies even in different domains, especially in the ones related to robot– or computer–human interaction.

## 6.2 Sensing within Soft Bodies

A first series of experiments has been carried out in order to provide an insight on the feasibility to use an EIT based touch sensor in order to identify the presence of inhomogeneities within soft material. The use of EIT in medical applications has been largely used especially to monitor functional changes, e.g. patient lung ventilation, or to observe the internal structure of the human body when other imaging technique were not available.

In this experiment, EIT imaging has been applied on a conductive textile in order to develop a tactile display that can be used in future medical applications alone or in combination with the ones already used, e.g. ultrasounds imaging. The imaging processing remains the same an in traditional EIT but, as it will be present later in this section, instead of applying direct force the responsive forces are detected. This will allow to detect stiffer structure within the soft body over which the technique is applied.

### 6.2.1 Experimental Setup and Protocol

Differently from the previous case, in order to test the feasibility of this application, a different experimental setup has been used. While the hardware used remains the same as in the previous experiments,
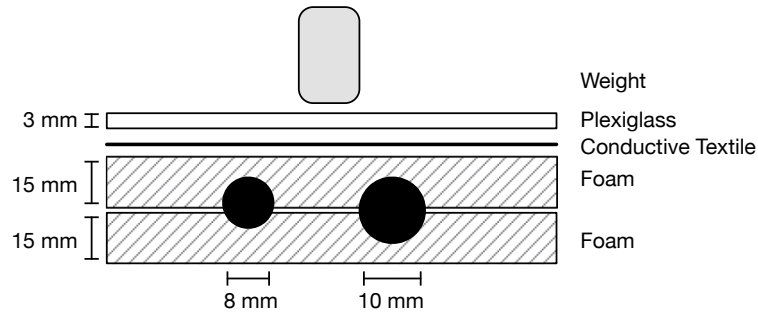
FIGURE 6.1: A schematic representation of the experimental setup. Two rigid bodies were placed within the soft phantom to simulate the presence of tumours.

the domain over which the measurements have been taken changes. Here, we developed a phantom that resembles a soft organ with the possibility to include stiffer element to simulate the presence of tumours.

The experimental setup consists of two layers of foam (100x100x15mm) within which a more rigid material—a medium-size marble—has been placed to simulate the presence of a tumour. The top layer has then been covered with a highly conductive textile (100x100mm) connected to the EIT system. To provide a homogenous pressure over the whole domain, an additional rigid layer (90x90x3mm) and a weight that is used to apply a constant force over the whole structure. The applied force deform the soft body and produce a reactive force from the stiffer elements placed within the soft substrates. Even though the developed experimental setup is minimal, results suggests that was sufficient to prove the feasibility of the method. Figure 6.1 shows the schematic representation of the described experimental setup.

Before attempting direct measurements over the experimental setup, various simulations have been performed in order to select the optimal parameters to be used in the different phases of the data acquisition process. Once the parameter are set, the measuring system is connected to the conductive textile that covered the soft. A constant force of 2N has been applied and as a consequence, the underlying soft structure has deformed. On the contrary, the stiff components do not deform but apply a normal force toward the conductive textile as a response to the applied force. This deform the conductive textile and change locally its resistance. These changes can be captured by EIT. In order to have a reliable analysis, measurements were taken ten times and then averaged. As in the previous cases, the experimental setup was placed over a flat rigid surface in order to not add interferences to the reconstructed image.
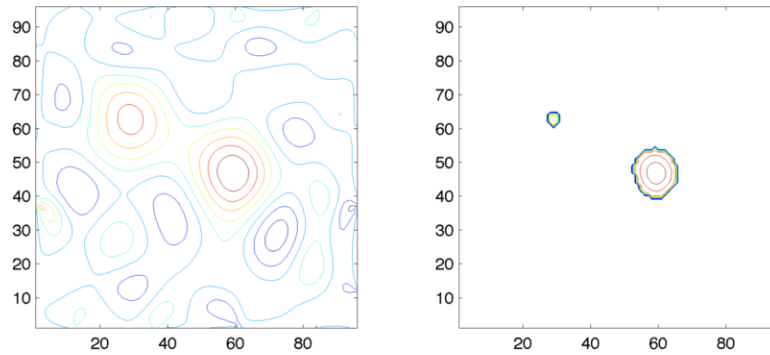
FIGURE 6.2: Results of the proposed method presented as contour map. (a) Reconstructed image. (b) Region having intensity value more than 75% of the maximum value detected. These regions represent the tumour inside the studied media

### 6.2.2 Results

Using the described experimental setup, we perform different measurements. Figure 6.2(a) shows the results obtained in the case where two stiff material of 10mm and 8mm, respectively, were introduced to simulate the presence of tumours. As the results suggest, the system was able to correctly identify the presence of the inhomogeneities and their position. Figure 6.2(b), instead, shows a simplified representation of the same results. This has been obtained with a threshold with respect to the maximum value detected over the image. For this reason the two inhomogeneities that were clearly distinguishable also in size the the previous image, here result to be less accurate.

## 6.3 EIT as Sensor for Tracking Facial Expressions

Following the results obtained so far, the system has been tested on a natural soft, deformable material such human skin. EIT has been used to sense within the internal structure of the human body, but not as a tool to track deformation that happen over its surface. In addition to EIT, other measurement methods—such as EMG or bio-impedance—have been used to track changes that occur over the human body. However, these suffers from within-subject reliability and within-measurements repeatability. EIT can have the same issues, let's think about the variability of the results caused by the simple movement of any of the electrodes, but is can be might used in combination with the other technique in order to increase its accuracy.

In this series of experiments, we are interested in detecting large changes in the morphology of the underlying structure by exploiting
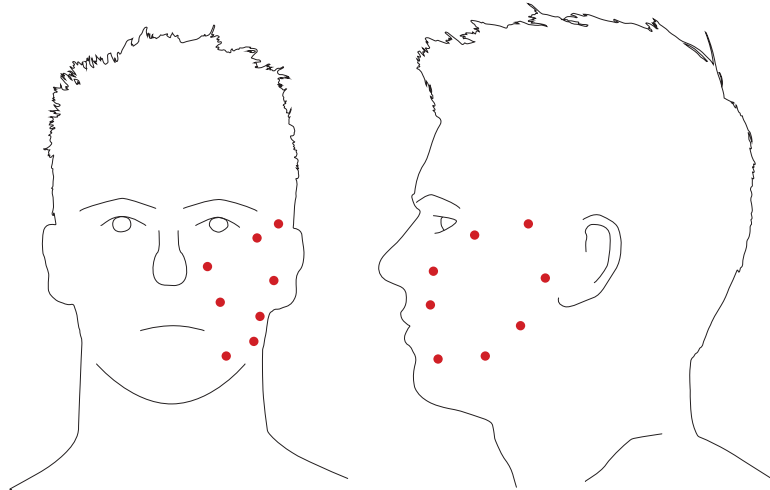
FIGURE 6.3: Electrode (red dots) placement over human face both in the front and side view.

the fact that *changes in the electrodes positioning generates error in the measurements*. By classifying such behaviour it is possible to recognise different facial expression, and thus use this technique as measurement system to evaluate rehabilitation treatments.

In order to test the capability of the system in performing the task, we tested it over a single volunteer that was trained to perform "wide" facial motion while reproducing the file vocal sound, and a full-face smile.

## 6.3.1   Experimental Setup and Protocol

In this series of experiment, we tuned the experimental hardware by controlling the frequency and the current amplitude to be injected into the tissue in order to follow the IEC-60601 standard and thus do not injure the volunteers. Despite this, the hardware and software configuration remains the same. Electrodes have been attached to the volunteer face using Ag/AgCl adhesive electrode directly connected to the system. No probe has been used during these tests, the reconstructed images has been obtained by comparing a reference "relaxed" position with later ones where the volunteers have been asked to change facial expression as earlier discussed. Figure 6.3 shows the ideal position of the electrodes over the face, and their application over the volunteer's face.

An in the previous cases, before attempting real measurements, a series of simulation have been carried out in order to correctly tune the parameters of the inverse solver. Once the electrode have been placed over the volunteer's face, a DC current of 2Vpp and 1mA has been injected into the system using an adjacent pattern.
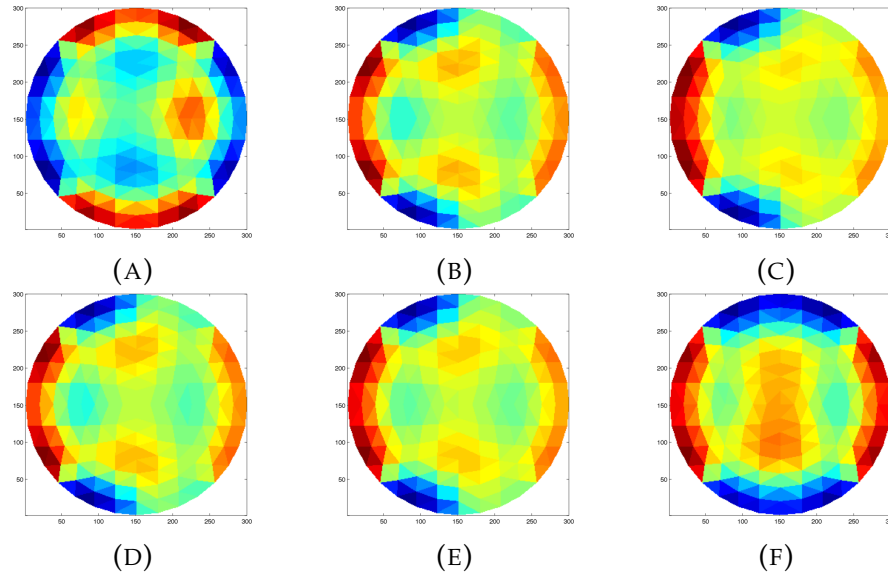
FIGURE 6.4: Result of the proposed method when applied over human skin. Each image represents the reconstructed conductivity map associated to the (A) "A" sound, (B) "E" sound, (C) "I" sound, (D) "O" sound, (E) "U" sound, and (F) "smile" expression. As the results suggest, only (A) and (F) are easily distinguishable from the maps since they show distinct features. The remaining are different in the means of small numerical fluctuation but these are not enough to clearly distinguish between the different events.

## 6.3.2 Results

The results are only preliminary and further investigation has to be performed. Nevertheless, as shown in Figure 6.4, the system is capable to grab the human skin deformations. Compare to the previous results, it is possible to notice a large noise especially around the boundaries. This is caused by the movement of the electrodes during the deformation process. As a consequence, the model used during the calibration and the one used for the measurements do not match causing this type of noise. However, these information can be used to discriminate which electrodes have been moved and which not allowing to discriminate between the different facial expressions. The use of DC current could have influenced the results since only the resistive components can be analysed. To improve the solution and AC based system should be implemented. Using this current solution only large deformations can be detected as consequence of change in the electrode position. Even if the system was able to reconstruct the conductivity map only in every situations, only the "A" and "smile" expressions show distinctive feature that can be used to discriminate between them.

# Chapter 7

# Discussion

We have demonstrated in a series of experiments the feasibility of the proposed EIT based deformable sensor. The results obtained from the respective experiments will be discussed in here with their implication, justification, and limitations. Some of the experiments and proof of concept trials mentioned in Chapter 5 will not be discussed here since their objective was simply to serve as basic testing of the proposal conducted throughout the development stage.

## 7.1  Indentation Test

A first series of experiments was performed to characterise the behaviour of the artificial skin. Concerning the specific results obtained in the indentation tests are the ones presented in Chapter 5. In these it is possible to notice a common pattern in the variation of the acquired signal as a consequence of the presence of a probe (in this specific case a 15mm circular section one) that applies a force in the region directly facing one of the electrodes under test. In order to understand the changes in the readings it was needed to compute the absolute variation of the electric potential with respect to a reference voltage ($V_{meas} - V_0$) that was acquired when no probe was acting on the conductive surface. By analysing these, the presence of the inhomogeneity can be noticed as a drop in the electric potentials measured at the electrode under test. The variation s caused by the change in conductivity of the conductive layer used for sensing as a consequence of the normal force applied over it. The variation is caused by the change in conductivity of the conductive layer used for sensing as a consequence of the normal force applied over it.

Considering the same electrode configuration, we evaluate the changes in the absolute voltage variation as a function of the probe size while applying a constant force (5 N) over them. Three different circular probes with radius of 15mm, 18mm, and 25mm were placed independently in front of the region facing one of the electrode. As the results suggest, with the increase of the probe size, the variations of the voltage potential increase. The phenomena was expected since a larger probe generates a wider inhomogeneity area that is the cause a consequent voltage drop. Even though it is possible to map probe size with the change in the electric potential, the same results can be

generated by using a single probe and apply an incremental pressure.

## 7.2   Pressure Map Reconstruction

Following the obtained results, we move toward the evaluation of the conductivity map reconstruction algorithm. To prove its effectiveness, we test the system under different configurations, in which we applied different probes independently or simultaneously over the artificial skin. The reconstructed pressure map (which is equivalent to the conductive map of the domain under study) was obtained by solving the associated inverse problem using a dynamic imaging approach. This consists of comparing a reference reading taken when no load was applied over the surface with a later one where a force was applied. Since the EIT inverse problem is ill-posed and ill-conditioned, in order to ensure uniqueness of the solution, it is needed to regularise the model during the inverse problem solution. Parameters to correctly tune the solver were selected after a series of trial and error experiments, and have been proved to be appropriate by evaluating them under different system configurations. It is worth noting that we kept the parameters constant in all experiments. Because of the low number of emitters and detectors used to build the electronic skin tested in this work, we did not expect a good spatial resolution for the contacts applied over the sensing area. Despite this, results provided show that the inverse solver can correctly identify the position of the applied force, but could not clearly identify its shape. To have a sharper identification of such area, we further process the data by thresholding it, identifying the pixels having value up to 70% of the maximum value present in the map. Considering the limitations due to the low resolution, we further test the system capabilities to discriminate between different probe sizes and shapes. As the reconstructed images suggest, the system is not able to correctly discriminate between different probe shapes (i.e., circular and square head), but it is able to correctly capture the differences in size (i.e., 15 mm, 18 mm, 25 mm for the circular probe, and 15 mm side for the square-headed probe).

## 7.3   Multi-Pressure Test on Hard Substrate

As a last test for this series of experiments, we evaluated the capability of the system to determine the presence and position of multiple probes that act sequentially and simultaneously over the sensing area of the artificial skin. For this series of experiments, we used three identical probes (circular section with radius of 15 mm) that were loaded and unloaded in the same order. In the results presented, it is possible to clearly distinguish the area where the probes

act, but due to the low spatial resolution, it is not possible to correctly identify their shapes. In addition, when all the probes were placed over the surface, in order to detect their positions, we had to change the value of the thresholding parameter used in the image segmentation. The use of a larger number of components, along with the introduction of more advanced coupling schemes for emitter–detector pairs can in the future improve the spatial performance and thus overcome some of the problems that the system is currently facing.

## 7.4 Application over Curved and Deformable Surfaces

We further tested the capabilities of the artificial skin by evaluating its ability to adapt to different geometries while maintaining its sensing performance. In the first phase, we tested the system's ability to detect a change in the underlying geometry caused by a significant change in the potential measurements. We first acquired a series of electric potentials with the artificial skin placed over a flat surface, and then manually placed it over a curved one. As curved surfaces, we used two different cylindrical objects with radii 40 mm and 70 mm, respectively. As the results indicate, when compared to the reconstructed images from the flat cases, the reconstructed images show a different "shape". These results, together with the fact that the maximum detected value and the size of the "deformation area" increased with respect to the radius of the underlaying cylinder, can be used as a clue to discriminate between different events (i.e., bending vs. touch) and their intensity (e.g., bending angles). Additionally, we tested the sensing capabilities of the system to provide reliable pressure readings when subjected to large deformations. In order to prove this, we tightly attached the artificial skin to objects having different shapes, and then performed pressure sensing. Contrary to the precious case, we acquired both the reference measurements and the later ones when the artificial skin was already placed over each object. Doing so, all of the deformations that occur as a consequence of the underlying geometries are negligible, since they are already taken into consideration in the reference measurements. As the results suggest, the system maintains its sensing capabilities and can identify the position where the probe was applied. Some issues were noticed when the sensor was applied over the mannequin, especially in the joint area. If the joint is moved after acquiring the initial reference measurements, the measurements acquired later are affected by a planar force applied by the joint—i.e., the joint stretching the material. The sensor can be still used in this situation by taking new reference measurements according to the information provided by

the joint encoder. For all the other cases, results remain valid, even when the probe was applied over the most bended area.

## 7.5   Sensing within Soft Bodies

We further stressed the idea of detecting different stimuli by using the EIT based sensor by applying it to a soft deformable structure. The conductive textile has been placed over a in-house developed medical phantom consisting in two layers of foam (100x100x15mm) within which a more rigid material—a medium-size marble—has been placed to simulate the presence of a tumour. The top layer has then been covered with a highly conductive textile (100x100mm) connected to the EIT system. To provide a homogenous pressure over the whole domain, an additional rigid layer (90x90x3mm) and a weight that is used to apply a constant force over the whole structure. A constant pressure has been applied to the structure and the response force from the internal stiff material has been acquired. As the results suggest, the system was able to correctly identify the presence of the inhomogeneities and their position. The experiment offers an insight on possible application in the medical field especially related to palpation of soft tissue. The technique can be used together, or alone and if minimised can be easily included within generic medical tools or into the ones used for minimal invasive surgery.

## 7.6   Sensing Natural Soft Material

A last series of experiments has been carried out in order to prove the capability of the system to adapt to different material, and in the specific to a natural soft material like human skin. When applied to a human face, the system has been tested without applying a direct force with any probe, the reconstructed images has been obtained by comparing a reference "relaxed" position with later ones where the volunteers have been asked to change facial expression. Due to the use of DC current instead of AC, and to limitation in the current hardware only large deformation, such as vocal sounds and full-face smile, were detected. Even if the system was able to reconstruct the conductivity map only in every situations, only the "A" and "smile" expressions show distinctive feature that can be used to discriminate between them. The results provide an insight on possible applications of this technique not only in human-computer interaction, but also as measurement tool for medical applications. EIT has been already used to measure the internal structure but using the proposed approach it can be used, alone or in combination with other technique such as EMG, to measure changes in the underlying structure. This feature can be used to track these changes and thus provide measurements that can be used to evaluate rehabilitation procedure.

# Chapter 8

# Conclusions and Future Works

In this research we explored and realised an Electrical Impedance Tomography (EIT) based sensor that has been used to detect deformations over soft and flexible materials.

Since the beginning of the work, it has been chosen to develop all the required components in-house. This was due not because of a luck of off the shelves technologies, but to have the full control o the single phase of the data acquisition and image processing. In addition, this allowed us to develop a more compact system than the one currently available on the marker that can be used in different situations.

We verified the proposed method and developed system through a series of experiments where it was applied under different configurations and scenarios. The implementation demonstrated the ability of the system in providing the correct location, in the cm range, of the applied external stimuli and it show the ability to discriminate between them. Additional tests have been performed to prove the capability of the system to adapt to different rigid, semi-rigid, and soft substrate. In the later case we also test the capability of the system in detecting change of the underlying structure. A last series of experiments has been carried out on a natural soft, and deformable material such as the human skin. The system, even with the intrinsic limitations due to the technique used, proved to be effective, and reliable as similar developed systems.

## 8.1   Contribution of This Work

The main contribution of the work is to introduce the Electrical Impedance Tomography to the field of deformable structure. This approach can be used in futuristic application such the ones involving the *soft robotic* filed where there are strong requirements on the deformability and adaptability of the technology used to develop these robotic devices. The use of this technique allows continuous distributed sensing without the need of active components directly embedded inside or beneath the sensing area. A direct consequence of the use of this approach is the simplification of the fabrication process (the sensing area can be any conductive material) and a smooth

extension to higher resolution. In addition, not having connecting cables that sit in the sensing area allows the developed of smart skins that can have a wider surface and that can easily adapt to different substrates and shapes. These are features that are not always achievable with the classical transduction methods. Moreover, an important aspect is the one related to the architecture used in the system. In fact, in order to increase the spatial resolution, the number of active components increases linearly with the length of the sensing area boundary, rather than with its area. This can be proven to be advantageous in terms of both costs and power consumption. On the contrary, the increase of active components places a larger burden in terms of computation time for the voltage acquisition system.

While the concept of EIT based sensing has been already exploited to create sensing structure in the past, the main application were limited to touch detection over stiff substrate. Here, the developed sensor structure presents additional system simplifications and hardware modularity that allows it to be more easily applied in situations where not only the sensor should adapt to different geometries, but also the underlying structure can change its shape.

## 8.2  Future Directions

Future works include the development of a larger electronic skin with higher density of active components, while keeping the focus on fast processing for real-time applications by exploring different coupling schemes. Additional work should also be done on the hardware side, by adding a signal conditioning stage to ensure more precise measurements. Another method to increase the system performance is to couple the current sensing methodology with capacitive measurements. This method has proved [67] to performs better than resistive both in detecting conductive an non-conductive objects. Since this sensor offers properties needed in the domain of soft robotics, we are currently investigating novel materials to be used as conductive layers that have similar properties to the one used in this work. In fact, the use of textiles is not suitable, since it is not possible to firmly attach them onto the material used to build such devices (i.e., silicon rubber).

Additional work have to be performed in order to fully exploit the EIT capability in the field of medical devices. In the specific, there is the need to convert the system from DC current to the AC once. This is needed since human skin does not behave simply like a variable resistor (like in the case of the conductive textile) but it shows a more complex behaviour that can be modelled with a combination of resistors and capacitors. The current use of DC current alone can not completely grab the changes of impedance of the human skin and thus all future application may result limited.

Looking to possible future applications, the developed sensor provide some essential functionalities not only for the field mentioned before, but also thanks to the results provided the sensing capability can be applied in other field where it is important to understand the changes in the morphology of the underlying structure without effecting it. Among these the ones that are the most straightforward to implement are those related to human-robot interaction. The use of EIT based sensing can bring interfaces that deform under the used action and thus provide a more natural feeling. In addition, the same technology can be applied to artificial limbs in order to provide tactile information to those robotic devices and thus let the user feel them. An additional field that can gain advantages by incorporating EIT based sensing is the one related to the development of medical tools. Among these, remote tactile display, or sensors for deformable endoscope are the ones that can benefit the most.

# Bibliography

[1] M.H Lee and H.R Nicholls. "Review Article Tactile sensing for mechatronics – a state of the art survey". In: *Mechatronics* 9.1 (1999), pp. 1 –31.

[2] Zhanat Kappassov, Juan-Antonio Corrales, and Véronique Perdereau. "Tactile Sensing in Dexterous Robot Hands - Review". In: *Robot. Auton. Syst.* 74.PA (Dec. 2015), pp. 195–220.

[3] David Silvera-Tawil, David Rye, and Mari Velonaki. "Artificial skin and tactile sensing for socially interactive robots: A review". In: *Robotics and Autonomous Systems* 63, Part 3 (2015). Advances in Tactile Sensing and Touch-based Human Robot Interaction, pp. 230 –243.

[4] Chiara Lucarotti, Calogero Maria Oddo, Nicola Vitiello, and Maria Chiara Carrozza. "Synthetic and Bio-Artificial Tactile Sensing: A Review". In: *Sensors* 13.2 (2013), p. 1435.

[5] R. Wijesiriwardana, K. Mitcham, W. Hurley, and T. Dias. "Capacitive fiber-meshed transducers for touch and proximity-sensing applications". In: *IEEE Sensors Journal* 5.5 (2005), pp. 989–994.

[6] A. Ueno, Y. Akabane, T. Kato, H. Hoshino, S. Kataoka, and Y. Ishiyama. "Capacitive Sensing of Electrocardiographic Potential Through Cloth From the Dorsal Surface of the Body in a Supine Position: A Preliminary Study". In: *IEEE Transactions on Biomedical Engineering* 54.4 (2007), pp. 759–766.

[7] Joseph C. Doll, Sung-Jin Park, and Beth L. Pruitt. "Design optimization of piezoresistive cantilevers for force sensing in air and water". In: *Journal of Applied Physics* 106.6 (2009), p. 064310.

[8] H. H. Gharib and W. A. Moussa. "On the Feasibility of a New Approach for Developing a Piezoresistive 3D Stress Sensing Rosette". In: *IEEE Sensors Journal* 11.9 (2011), pp. 1861–1871.

[9] J. Missinne, E. Bosman, B. Van Hoe, G. Van Steenberge, P. Van Daele, and J. Vanfleteren. "Embedded flexible optical shear sensor". In: *Sensors, 2010 IEEE*. 2010, pp. 987–990.

[10] Alessandro Levi, Matteo Piovanelli, Silvano Furlan, Barbara Mazzolai, and Lucia Beccai. "Soft, Transparent, Electronic Skin for Distributed and Multiple Pressure Sensing". In: *Sensors* 13.5 (2013), p. 6578.

[11] Y. H. Wen, G. Y. Yang, V. J. Bailey, G. Lin, W. C. Tang, and J. H. Keyak. "Mechanically robust micro-fabricated strain gauges for use on bones". In: *2005 3rd IEEE/EMBS Special Topic Conference on Microtechnology in Medicine and Biology*. 2005, pp. 302–304.

[12] Y. Kim, Y. Kim, C. Lee, and S. Kwon. "Thin Polysilicon Gauge for Strain Measurement of Structural Elements". In: *IEEE Sensors Journal* 10.8 (2010), pp. 1320–1327.

[13] H. Ruser. "Smartlow-cost weather sensor as an example for 'multi-component' sensors". In: *2006 IEEE International Conference on Multisensor Fusion and Integration for Intelligent Systems*. 2006, pp. 559–564.

[14] J. H. Cho, M. Kothare, and M. G. Arnold. "Reconfigurable multi-component sensors built from MEMS payloads carried by micro-robots". In: *2010 IEEE Sensors Applications Symposium (SAS)*. 2010, pp. 15–19.

[15] K. S. Jaichandar and E. A. M. García. "Intelli-sense bed patient movement sensing and anti-sweating system for bed sore prevention in a clinical environment". In: *2011 8th International Conference on Information, Communications Signal Processing*. 2011, pp. 1–5.

[16] Fumiya Iida and Cecilia Laschi. "Soft Robotics: Challenges and Perspectives". In: *Procedia Computer Science* 7 (Jan. 2011), pp. 99–102.

[17] Rolf Pfeifer, Max Lungarella, and Fumiya Iida. "The challenges ahead for bio-inspired'soft'robotics". In: *Communications of the ACM* 55.11 (Nov. 2012), p. 76.

[18] J E Molyneux and A Witten. "Impedance tomography: imaging algorithms for geophysical applications". In: *Inverse Problems* 10.3 (1994), p. 655.

[19] Chang Seop Koh, Min-Kyu Kim, Hyun-Kyo Jung, Song yop Hahn, and Baek soo Suh. "Electric resistivity tomography for geophysical inverse problems". In: *IEEE Transactions on Magnetics* 33.2 (1997), pp. 1852–1855.

[20] Richard H Bayford and Bill R B Lionheart. "Biomedical applications of electrical impedance tomography". In: *Physiological Measurement* 25.1 (2004).

[21] M. T. Erwati and N. Farrukh. "Application of electrical impedance tomography for imaging in bio-medical and material technology". In: *Research and Development (SCOReD), 2009 IEEE Student Conference on*. 2009, pp. 168–171.

[22] A. Nagakubo, H. Alirezaei, and Y. Kuniyoshi. "A deformable and deformation sensitive tactile distribution sensor". In: *Robotics and Biomimetics, 2007. ROBIO 2007. IEEE International Conference on*. 2007, pp. 1301–1308.

[23] Y. Kato, T. Mukai, T. Hayakawa, and T. Shibata. "Tactile Sensor without Wire and Sensing Element in the Tactile Region Based on EIT Method". In: *Sensors, 2007 IEEE*. 2007, pp. 792–795.

[24] David Silvera Tawil, David Rye, and Mari Velonaki. "Interpretation of the Modality of Touch on an Artificial Arm Covered with an EIT-based Sensitive Skin". In: *The International Journal of Robotics Research* (2012).

[25] M. D. Cooney, S. Nishio, and H. Ishiguro. "Recognizing affection for a touch-based interaction with a humanoid robot". In: *2012 IEEE/RSJ International Conference on Intelligent Robots and Systems*. 2012, pp. 1420–1427.

[26] A. Yao and M. Soleimani. "A pressure mapping imaging device based on electrical impedance tomography of conductive fabrics". In: *Sensor Review* 32.4 (2012), pp. 310–317.

[27] A. Yao, C. L. Yang, J. K. Seo, and M. Soleimani. "EIT-Based Fabric Pressure Sensing". In: *Computational and Mathematical Methods in Medicine* 2013 (2013), p. 9.

[28] David S. Holder. *Electrical Impedance Tomography: Methods, History and Applications*. CRC Press, 2004.

[29] RHT Bates, Kathryn L Garden, and Terence M Peters. "Overview of computerized tomography with emphasis on future developments". In: *Proceedings of the IEEE* 71.3 (1983), pp. 356–372.

[30] R. P. Henderson and J. G. Webster. "An Impedance Camera for Spatially Specific Measurements of the Thorax". In: *IEEE Transactions on Biomedical Engineering* BME-25.3 (1978), pp. 250–254.

[31] D C Barber and B H Brown. "Applied potential tomography". In: *Journal of Physics E: Scientific Instruments* 17.9 (1984), p. 723.

[32] Fraser Dickin and Mi Wang. "Electrical resistance tomography for process applications". In: *Measurement Science and Technology* 7.3 (1996), p. 247.

[33] Giovanni Alessandrini and Luca Rondi. "Stable Determination of a Crack in a Planar Inhomogeneous Conductor". In: *SIAM Journal on Mathematical Analysis* 30.2 (1999), pp. 326–340.

[34] Milad Hallaji, Aku Seppänen, and Mohammad Pour-Ghaz. "Electrical impedance tomography-based sensing skin for quantitative imaging of damage in concrete". In: *Smart Materials and Structures* 23.8 (2014), p. 085001.

[35] MH Loke. "Electrical imaging surveys for environmental and engineering studies". In: *A practical guide to* 2 (1999).

[36] B. M. Eyuboglu, B. H. Brown, and D. C. Barber. "In vivo imaging of cardiac related impedance changes". In: *IEEE Engineering in Medicine and Biology Magazine* 8.1 (1989), pp. 39–45.

[37] D. S. Holder. "Electrical impedance tomography (EIT) of brain function". In: *Brain Topography* 5.2 (1992), pp. 87–93.

[38] R H Smallwood, Y F Mangnall, and A D Leathard. "Transport of gastric contents (electric impedance imaging)". In: *Physiological Measurement* 15.2A (1994), A175.

[39] I. Frerichs, G. Hahn, and G. Hellige. "Thoracic electrical impedance tomographic measurements during volume controlled ventilation-effects of tidal volume and positive end-expiratory pressure". In: *IEEE Transactions on Medical Imaging* 18.9 (1999), pp. 764–773.

[40] G Uhlmann. "Electrical impedance tomography and Calderón's problem". In: *Inverse Problems* 25.12 (2009), p. 123011.

[41] G. Blumrosen, C. A. Gonzalez, and B. Rubinsky. "New Wearable Body Sensor for Continuous Diagnosis of Internal Tissue Bleeding". In: *2009 Sixth International Workshop on Wearable and Implantable Body Sensor Networks*. 2009, pp. 120–124.

[42] Manuchehr Soleimani, Cathryn N Mitchell, R Banasiak, R Wajman, and A Adler. "Four-dimensional electrical capacitance tomography imaging using experimental data". In: *Progress In Electromagnetics Research (PIER)* 90 (2009), pp. 171–186.

[43] H.S. Tapp, A.J. Peyton, E.K. Kemsley, and R.H. Wilson. "Chemical engineering applications of electrical process tomography". In: *Sensors and Actuators B: Chemical* 92.1–2 (2003), pp. 17 –24.

[44] Jari Kourunen, Ritva Käyhkö, Jouni Matula, Jari Käyhkö, Marko Vauhkonen, and Lasse M. Heikkinen. "Imaging of mixing of two miscible liquids using electrical impedance tomography and linear impedance sensor". In: *Flow Measurement and Instrumentation* 19.6 (2008), pp. 391 –396.

[45] H. P. Schwan. "Electrical properties of tissues and cell suspensions: mechanisms and models". In: *Proceedings of 16th Annual International Conference of the IEEE Engineering in Medicine and Biology Society*. 1994, A70–A71 vol.1.

[46] J. Jossinet. "Variability of impedivity in normal and pathological breast tissue". In: *Medical and Biological Engineering and Computing* 34.5 (1996), pp. 346–350.

[47] A. J. Surowiec, S. S. Stuchly, J. R. Barr, and A. Swarup. "Dielectric properties of breast carcinoma and the surrounding tissues". In: *IEEE Transactions on Biomedical Engineering* 35.4 (1988), pp. 257–263.

[48] W. S. Fulton and R. T. Lipczynski. "Body-support pressure measurement using electrical impedance tomography". In: *Proceedings of the 15th Annual International Conference of the IEEE Engineering in Medicine and Biology Societ*. 1993, pp. 98–99.

[49] H. Alirezaei, A. Nagakubo, and Y. Kuniyoshi. "A tactile distribution sensor which enables stable measurement under high and dynamic stretch". In: *3D User Interfaces, 2009. 3DUI 2009. IEEE Symposium on*. 2009, pp. 87–93.

[50] David Silvera-Tawil, David Rye, and Mari Velonaki. "Interpretation of Social Touch on an Artificial Arm Covered with an EIT-based Sensitive Skin". In: *International Journal of Social Robotics* 6.4 (2014), pp. 489–505.

[51] A. Adler and R. Guardo. "Electrical impedance tomography: regularized imaging and contrast detection". In: *IEEE Transactions on Medical Imaging* 15.2 (1996), pp. 170–179.

[52] A. Adler, R. Guardo, and Y. Berthiaume. "Impedance imaging of lung ventilation: do we need to account for chest expansion?" In: *IEEE Transactions on Biomedical Engineering* 43.4 (1996), pp. 414–420.

[53] Marko Vauhkonen. *Electrical impedance tomography and prior information*. 1997.

[54] G. Boverman, B. S. Kim, D. Isaacson, and J. C. Newell. "The Complete Electrode Model For Imaging and Electrode Contact Compensation in Electrical Impedance Tomography". In: *2007 29th Annual International Conference of the IEEE Engineering in Medicine and Biology Society*. 2007, pp. 3462–3465.

[55] R. H. T. Bates, G. C. Mckinnon, and A. D. Seagar. "A Limitation on Systems for Imaging Electrical Conductivity Distributions". In: *IEEE Transactions on Biomedical Engineering* BME-27.7 (1980), pp. 418–420.

[56] M. V. K. Chari, G. Bedrosian, J. D'Angelo, and A. Konrad. "Finite element applications in electrical engineering". In: *IEEE Transactions on Magnetics* 29.2 (1993), pp. 1306–1314.

[57] T. K. Bera and J. Nagaraju. "A FEM-Based Forward Solver for Studying the Forward Problem of Electrical Impedance Tomography (EIT) with A Practical Biological Phantom". In: *2009 IEEE International Advance Computing Conference*. 2009, pp. 1375–1381.

[58] P.P. Silvester and R.L. Ferrari. *Finite Elements for Electrical Engineers*. Cambridge University Press, 1983.

[59] M. Cheney and D. Isaacson. "Issues in electrical impedance imaging". In: *IEEE Computational Science and Engineering* 2.4 (1995), pp. 53–62.

[60]  A. Adler and R. Guardo. "Electrical impedance tomography: regularized imaging and contrast detection". In: *IEEE Transactions on Medical Imaging* 15.2 (1996), pp. 170–179.

[61]  B. M. Graham and A. Adler. "A nodal jacobian algorithm for reduced complexity EIT reconstructions". In: *International Journal of Systems Science* 2 (2006), pp. 453–456.

[62]  Andy Adler and William R B Lionheart. "Uses and abuses of EIDORS: an extensible software base for EIT". In: *Physiological Measurement* 27.5 (2006), S25.

[63]  M. Cheney, D. Isaacson, J. C. Newell, S. Simske, and J. Goble. "NOSER: An algorithm for solving the inverse conductivity problem". In: *International Journal of Imaging Systems and Technology* 2.2 (1990), pp. 66–75.

[64]  Andy Adler, John H Arnold, Richard Bayford, Andrea Borsic, Brian Brown, Paul Dixon, Theo J C Faes, Inéz Frerichs, Hervé Gagnon, Yvo Gärber, Bartłomiej Grychtol, Günter Hahn, William R B Lionheart, Anjum Malik, Robert P Patterson, Janet Stocks, Andrew Tizzard, Norbert Weiler, and Gerhard K Wolf. "GREIT: a unified approach to 2D linear EIT reconstruction of lung images". In: *Physiological Measurement* 30.6 (2009), S35.

[65]  James L Wheeler, Wei Wang, and Mengxing Tang. "A comparison of methods for measurement of spatial resolution in two-dimensional circular EIT images". In: *Physiological Measurement* 23.1 (2002), p. 169.

[66]  M. Cheney, D. Isaacson, J. C. Newell, S. Simske, and J. Goble. "NOSER: An algorithm for solving the inverse conductivity problem". In: *International Journal of Imaging Systems and Technology* 2.2 (1990), pp. 66–75.

[67]  Yang Bai, Izaak D Neveln, Michael Peshkin, and Malcolm A MacIver. "Enhanced detection performance in electrosense through capacitive sensing". In: *Bioinspiration & Biomimetics* 11.5 (2016), p. 055001.